Identification of unique SUN-interacting nuclear envelope proteins with diverse functions in plants

Xiao Zhou[1], Katja Graumann,[2] Lennart Wirthmueller,[3] Jonathan D.G. Jones,[3] and Iris Meier[1]

[1]Department of Molecular Genetics, The Ohio State University, Columbus, OH 43210
[2]Department of Biological and Medical Sciences, Faculty of Health and Life Sciences, Oxford Brookes University, Oxford OX3 OBP, England, UK
[3]The Sainsbury Laboratory, Norwich NR4 7UH, England, UK

Although a plethora of nuclear envelope (NE) transmembrane proteins (NETs) have been identified in opisthokonts, plant NETs are largely unknown. The only known NET homologues in plants are Sad1/UNC-84 (SUN) proteins, which bind Klarsicht/ANC-1/Syne-1 homology (KASH) proteins. Therefore, de novo identification of plant NETs is necessary. Based on similarities between opisthokont KASH proteins and the only known plant KASH proteins, WPP domain–interacting proteins, we used a computational method to identify the KASH subset of plant NETs. Ten potential plant KASH protein families were identified, and five candidates from four of these families were verified for their NE localization, depending on SUN domain interaction. Of those, *Arabidopsis thaliana* SINE1 is involved in actin-dependent nuclear positioning in guard cells, whereas its paralogue SINE2 contributes to innate immunity against an oomycete pathogen. This study dramatically expands our knowledge of plant KASH proteins and suggests that plants and opisthokonts have recruited different KASH proteins to perform NE regulatory functions.

Introduction

At the basic structural level, the nuclear envelope (NE) is a protective barrier of the genome. However, studies in opisthokonts have revealed that, at the molecular level, the NE is a regulatory platform containing NE transmembrane proteins (NETs) involved in nuclear positioning, nuclear mechanics (shape, volume, and rigidity), gene expression, and genome organization, which are essential for cell migration, stability, division, and proliferation (Mekhail and Moazed, 2010; Starr and Fridolfsson, 2010; Hampoelz and Lecuit, 2011; Zuleger et al., 2011b). However, the protein complement of the opisthokont NE appears to be largely missing from land plants, whereas several plant-unique NE proteins have been described (Meier, 2001; Gruenbaum et al., 2003; Xu et al., 2007; Zhao et al., 2008; Graumann and Evans, 2010). This is in stark contrast to the nuclear pore complex, which seems to have been established at the time of the last eukaryotic common ancestor (Neumann et al., 2010). In light of the fact that open mitosis has likely evolved at least twice (De Souza and Osmani, 2007; Meier et al., 2008; Becker and Marin, 2009), there may be a much deeper functional and compositional divide between opisthokont and land plant NEs. Identifying plant NETs is critical to resolve this enigma.

The NE linker of nucleoskeleton and cytoskeleton (LINC) complexes (Crisp et al., 2006) are formed by two types of NETs—inner nuclear membrane Sad1/UNC-84 (SUN) proteins and outer nuclear membrane Klarsicht/ANC-1/Syne-1 homology (KASH) proteins—through SUN–KASH domain interactions in the perinuclear space (Razafsky and Hodzic, 2009; Starr and Fridolfsson, 2010; Sosa et al., 2012; Zhou et al., 2012b). LINC complexes have been identified in multiple organisms and have been shown to play roles in nuclear positioning, nuclear shape, and chromatin–NE interactions (Razafsky and Hodzic, 2009; Starr and Fridolfsson, 2010; Mellad et al., 2011; Gundersen and Worman, 2013; Rothballer and Kutay, 2013). Mutations in SUN or KASH proteins lead to several developmental abnormalities

K. Graumann and L. Wirthmueller contributed equally to this paper.

Correspondence to Iris Meier: meier.56@osu.edu

Abbreviations used in this paper: ARM, armadillo; Ccdc155, coiled-coil domain-containing protein 155; GI, GenInfo Identifier; GUS, β-glucuronidase; *Hpa*, *Hyaloperonospora arabidopsidis*; IP, immunoprecipitation; KASH, Klarsicht/ANC-1/Syne-1 homology; KD, knockdown; KO, knockout; LatB, Latrunculin B; LINC, linker of nucleoskeleton and cytoskeleton; Lrmp, lymphoid-restricted membrane protein; NE, nuclear envelope; NES, nuclear export signal; NET, NE transmembrane protein; NLI, NE localization index; ROI, region of interest; SINE, SUN domain–interacting NE protein; SUN, Sad1/UNC-84; TAN, transmembrane actin-associated nuclear; T-DNA, transfer DNA; TMD, transmembrane domain; WIP, WPP domain–interacting protein; WIT, WPP domain–interacting tail-anchored protein.

The Rockefeller University Press $30.00
J. Cell Biol. Vol. 205 No. 5 677–692
www.jcb.org/cgi/doi/10.1083/jcb.201401138

and are implicated in human diseases (Malone et al., 1999; Starr et al., 2001; Zhang et al., 2009; Elhanany-Tamir et al., 2012; Schreiber and Kennedy, 2013).

SUN proteins are present in plants (Graumann et al., 2010; Oda and Fukuda, 2011), but no homologues of opisthokont KASH proteins can be identified in plant proteomes. Recently, AtWIPs (*Arabidopsis thaliana* WPP domain-interacting proteins [WIPs]) were identified as plant-specific KASH proteins (Zhou et al., 2012a). The AtSUN (*A. thaliana* SUN)–AtWIP complexes anchor plant RanGAP1 (Ran GTPase-activating protein 1) to the NE and are required for the elongated nuclear shape in epidermal cells. WIPs also interact with WPP domain–interacting tail-anchored proteins (WITs), and they synergistically anchor RanGAP1 to the NE (Zhao et al., 2008). Recent evidence shows that SUN–WIP–WIT–myosin XI-I complexes probably exist and regulate elongated nuclear shape and nuclear movement (Tamura et al., 2013), suggesting that LINC complexes are also conserved in plants, albeit with different components.

Based on detailed knowledge of opisthokont SUN–KASH complex formation (Sosa et al., 2012; Zhou et al., 2012b) and the known conservation of the KASH domains, we reasoned that a computational approach could be developed to discover unknown KASH proteins in plants and provide better understanding of the KASH subset of plant NETs. Here, we describe this approach and the experimental verification of five candidates from four protein families. We show that all five proteins are localized to the NE, and this localization depends on their interaction with the SUN domain of SUN proteins. Among the five proteins, *A. thaliana* SINE1 and SINE2 are conserved across land plants and have distinct expression profiles and functions in leaves. SINE1 is predominantly expressed in guard cells, is associated with F-actin, and is involved in centrally positioning guard cell nuclei, whereas SINE2 is predominantly expressed in other leaf cell types, shows no association with F-actin, and contributes to innate immunity against an oomycete pathogen.

Results

Identification of SUN domain–interacting NE protein candidates

Plant genomes do not encode any homologues of known opisthokont KASH proteins. The KASH domains of opisthokont KASH proteins and plant WIPs terminate in a C-terminal 4-aa motif (Fig. S1 A and Fig. S2 G), which is critical for interacting with the SUN domain and for NE localization (Padmakumar et al., 2005; Ketema et al., 2007; Morimoto et al., 2012; Sosa et al., 2012; Zhou et al., 2012a). However, the KASH domains of plant WIPs and of animal KASH proteins share little amino acid similarity. Even among plant WIPs, the composition of the KASH domain varies significantly, except for the C-terminal 4 aa and, in particular, the terminal PT (Fig. S1 A). Thus, we define a protein sequence as a putative KASH domain when it fulfills all of the following: (a) it is immediately C-terminal of a transmembrane domain (TMD); (b) its length is between 9 and 40 aa (based on animal KASH proteins and plant WIPs); and (c) it is the C terminus of a protein and terminates in four amino acids with a given amino acid pattern. A Java program called DORY was developed to search for putative KASH domain–containing proteins according to these rules (Fig. S1 B, flow chart). In addition, we argued that if a putative KASH domain is present in most members of a protein family, it is more likely to be a bona fide KASH domain. Therefore, BLASTP (Protein Basic Local Alignment Search Tool) was used to obtain homologues of a positive output from DORY in the NCBI nr (nonredundant) database (in this study, proteins with an expect (E)-value < 0.0001 are considered as homologues).

We first ran this method on the *A. thaliana* proteome using XXPT (X represents any amino acid) as the C-terminal 4-aa pattern. Four putative KASH candidates were identified—At1G54385.1, At3G03970.1, At3G06600.1, and At4G24950.1—and they are all plant specific (please see Materials and methods for details). At1G54385.1 and At3G03970.1 are paralogues in *A. thaliana* and are conserved across land plants (Fig. 1 A). At3G06600.1 has close homologues in *Arabidopsis lyrata* and in the closely related species *Capsella rubella* and has distant homologues in other dicots (Fig. 1 B). At4G24950.1 has only one homologue each in *A. lyrata* and *C. rubella* (Fig. 1 C).

Analyzing the last 4 aa of these five candidates and their homologues revealed a new pattern of [DTVAMPLIFY][VAPIL]PT (brackets indicate alternative amino acid residues at the respective position). This pattern was used to search the nr database for putative KASH proteins in plants. Seven new protein families were identified (Fig. 1 D and Fig. S2, A–F). The protein family shown in Fig. 1 D was identified only in *Medicago truncatula*, and one homologue was subsequently cloned from *Medicago sativa*. The protein families shown in Fig. S2 (A and B) were only found in *Poaceae*. This search also came across a mammalian protein family, T191C (transmembrane 191C), which has a conserved TMD followed by a short sequence (~40 aa) terminating in a conserved LLP[AST] motif (Fig. S2 G).

Among these candidates, we chose At1G54385.1, At3G03970.1, At3G06600.1, and At4G24950.1 for verification and named them SINE1, SINE2, SINE3, and SINE4, respectively, because of their putative SUN domain–binding properties and NE localizations. We also cloned a homologue of the protein family shown in Fig. 1 D from *M. sativa* (SINE5) for verification.

SINE1, SINE2, SINE3, SINE4, and SINE5 are localized to the plant NE

To determine the subcellular localization of the chosen plant KASH candidates, transgenic wild-type *A. thaliana* lines were generated that express N-terminally GFP-tagged proteins under the control of the Cauliflower Mosaic Virus 35S (35S) promoter. Root tip cells of 7–10-d-old seedlings were imaged by confocal microscopy, and at least three lines for each construct were analyzed. As shown in Fig. 2 A, all five fusion proteins were associated with the NE.

SINE1, SINE2, SINE3, SINE4, and SINE5 interact with AtSUN1 and AtSUN2

Next, we tested the ability of SINE1, SINE2, SINE3, SINE4, and SINE5 to interact with AtSUN1 and AtSUN2 (Fig. 3 and Fig. 4). Pairs of tagged proteins were transiently expressed

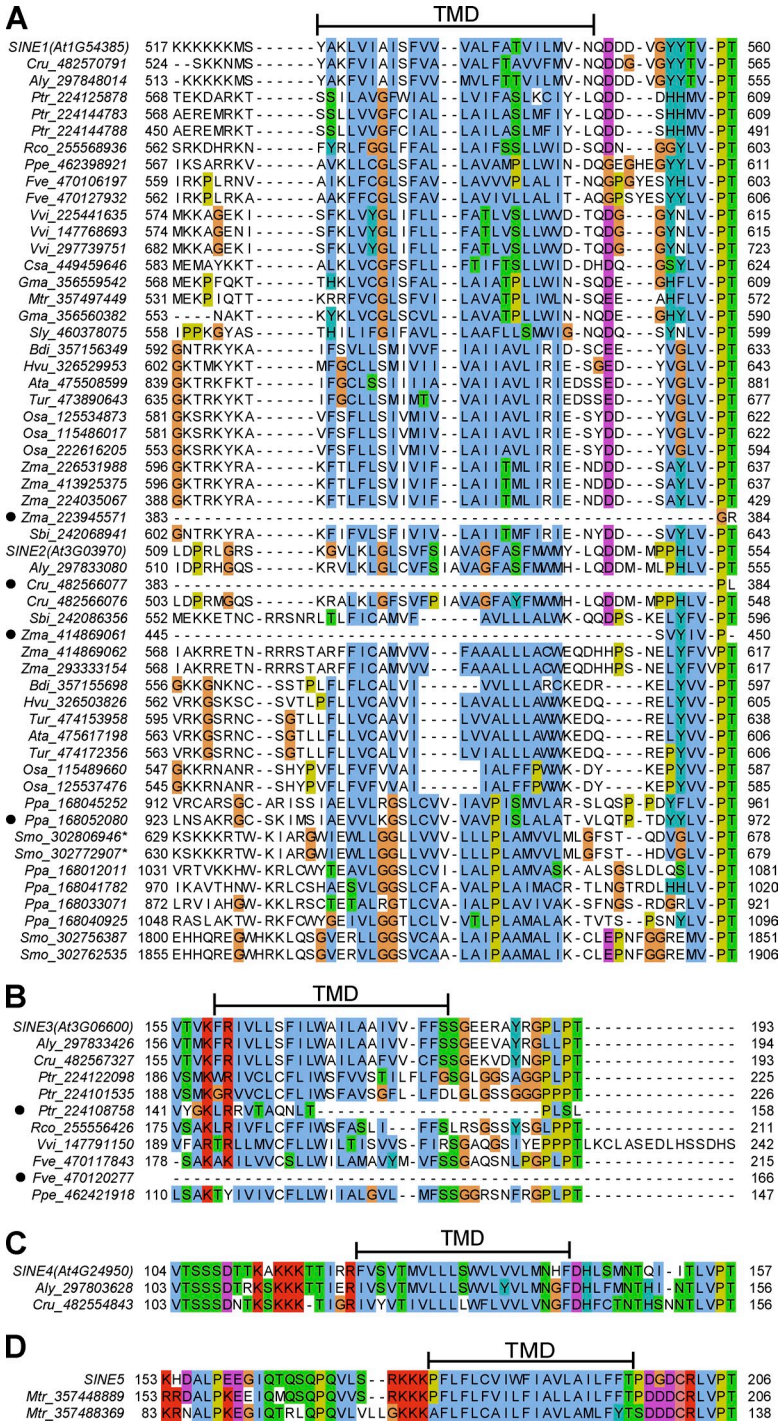

Figure 1. **Amino acid sequence alignment of the C-terminal domains of predicted plant KASH proteins.** (A–D) Amino acid sequence alignment of SINE1/2 homologues (A), SINE3 homologues (B), SINE4 homologues (C), and SINE5 homologues (D). Full-length protein sequences were used for the alignment, and only the C termini are shown. *Aly, A. lyrata; Ata, Aegilops tauschii; Bdi, Brachypodium distachyon; Cru, C. rubella; Csa, Cucumis sativus; Fve, Fragaria vesca; Gma, G. max; Hvu, Hordeum vulgare; Mtr, M. truncatula; Osa, Oryza sativa; Ppa, Physcomitrella patens; Ppe, Prunus persica; Ptr, Populus trichocarpa; Rco, Ricinus communis; Sbi, Sorghum bicolor; Sly, Solanum lycopersicum; Smo, S. moellendorffii; Tur, Triticum urartu; Vvi, V. vinifera; Zma, Zea mays.* The numbers after the abbreviations are GI numbers. Locus names of *A. thaliana* proteins are shown in parentheses. Asterisks indicate that the protein models were corrected according to the predicted TMD-putative KASH domain architecture in the ORFs (see Materials and methods for detail). Numbers at the edges of the alignment indicate the first and last (terminal) amino acids of the domains shown. The Phobius-predicted TMD of the first sequence in each alignment is indicated above the sequence. Filled circles indicate proteins predicted not to have a TMD by Phobius. ClustalX color was assigned to the alignments.

under the control of the 35S promoter in *Nicotiana benthamiana* leaves and coimmunoprecipitation (IP; co-IP) assays were performed. To determine the importance of the C-terminal 4 aa of each candidate, deletions of these amino acids were introduced, and the resulting mutant proteins were designated as SINE1ΔTVPT, SINE2ΔLVPT, SINE3ΔPLPT, SINE4ΔLVPT, and SINE5ΔLVPT, respectively (Fig. 3 A and Fig. 4 A). To test whether the putative KASH domains of SINE1, SINE2, and SINE3 are essential for SUN protein interaction, they were replaced with RFYTKSAEAAAAA (SINE1XT), RFYTKSAEAAAA (SINE2XT), and RFYTKSAEAAAAAA (SINE3XT), respectively (Fig. 3 A and Fig. 4 A). The underlined sequence is the luminal domain of the ER tail-anchored protein cytochrome *b5c* from *Aleurites fordii* (Hwang et al., 2004), lengthened with alanine residues to the size of the respective putative KASH domains.

GFP-SINE1, GFP-SINE1ΔTVPT, GFP-SINE1XT, GFP-SINE2, GFP-SINE2ΔLVPT, or GFP-SINE2XT was transiently coexpressed with N-terminally Myc-Flag–tagged AtSUN1 (Myc-Flag-AtSUN1). IP assays were performed with an anti-GFP antibody. As shown in Fig. 3 C, Myc-Flag-AtSUN1 was strongly coimmunoprecipitated with GFP-SINE1 or GFP-SINE2 but barely with GFP-SINE1ΔTVPT, GFP-SINE2ΔLVPT,

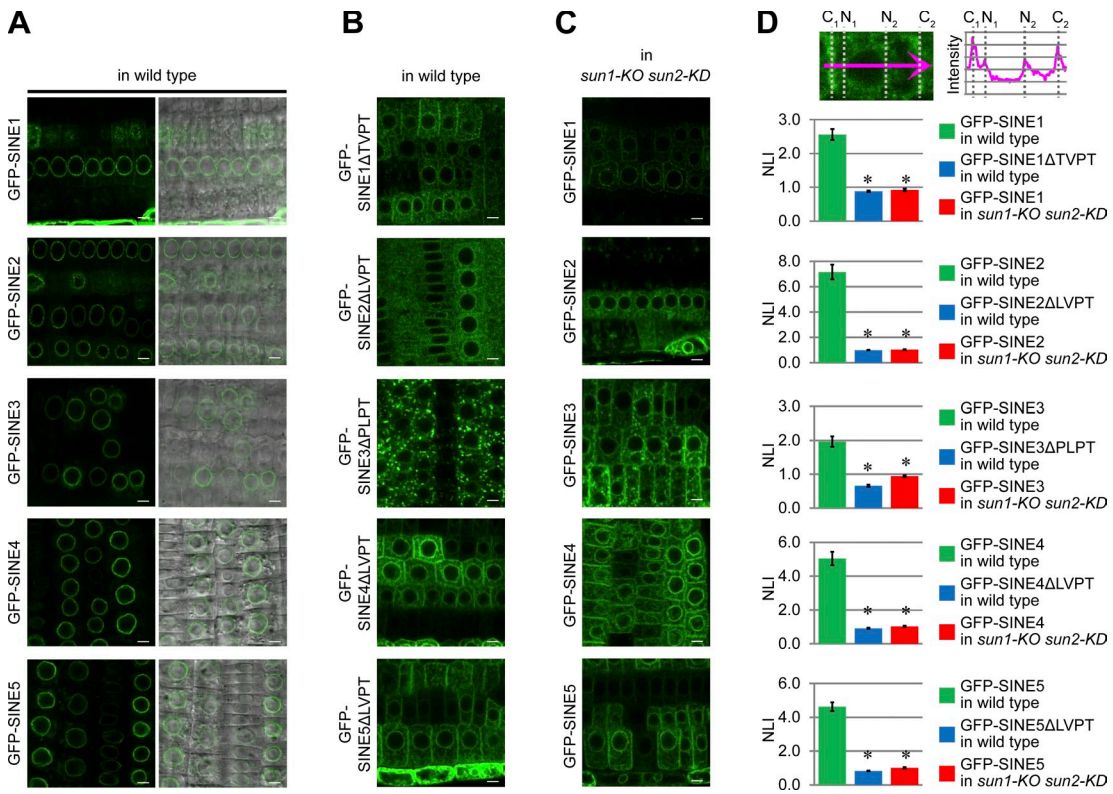

Figure 2. **Subcellular localization of predicted plant KASH proteins.** (A and C) GFP-tagged SINE1, SINE2, SINE3, SINE4, and SINE5 under control of the 35S promoter were stably expressed in wild type (A) or *sun1-KO sun2-KD* (C), respectively. (B) GFP-tagged SINE1ΔTVPT, SINE2ΔLVPT, SINE3ΔPLPT, SINE4ΔLVPT, and SINE5ΔLVPT driven by the 35S promoter were stably expressed in wild-type *A. thaliana*. Root tip cells were imaged using confocal microscopy. Bars, 5 µm. GFP signal is shown in green. Images in the second column of A are overlays of GFP and transmitted light images. Cell-to-cell variability of GFP fusion protein abundance was seen in all images. (D) The NLI was calculated and compared. As illustrated in the top of D, two maximum NE intensities (N_1 and N_2) and two maximum cytoplasmic intensities (C_1 and C_2) along a random line across a cell were chosen to calculate the NLI, which equals $(N_1 + N_2)/(C_1 + C_2)$. Asterisks in D represent significant statistic differences when compared with GFP-tagged wild-type SINEs in wild-type *A. thaliana* ($P < 0.01$, two-tailed *t* test, $n = 30$). Error bars show SEMs.

GFP-SINE1XT, or GFP-SINE2XT. A similar co-IP procedure was performed to test the interaction of Myc-AtSUN2 with SINE1, SINE2, and their respective mutants. As shown in Fig. 3 D, Myc-AtSUN2 was strongly coimmunoprecipitated with GFP-SINE1 or GFP-SINE2, weakly with GFP-SINE1ΔTVPT, and barely with GFP-SINE2ΔLVPT, GFP-SINE1XT, or GFP-SINE2XT. These data indicate that the putative KASH domain and the C-terminal 4 aa are important for AtSUN1 and AtSUN2 binding.

To test whether the SUN domain of AtSUN1 and AtSUN2 is necessary for this interaction, co-IP assays were performed with AtSUN2 deletion mutants (Fig. 3 B) and SINE1. Myc-SINE1 was coexpressed with CFP-AtSUN2, CFP-AtSUN2ΔN (deletion of the N-terminal 106 aa), CFP-AtSUN2ΔCC (deletion of the coiled-coil domain, aa 205–225), CFP-AtSUN2ΔCSUN (deletion of the C-terminal 146 aa of the SUN domain), and GFP-Myc-AtSUN2ΔNSUN (deletion of the N-terminal 84 aa of the SUN domain). As a negative control, the unrelated GFP-NLS-GFP–nuclear export signal (NES) fusion protein was used. After IP using an anti-GFP antibody, coimmunoprecipitated Myc-SINE1 was detected by an anti-Myc antibody. As shown in Fig. 3 E, only the two SUN domain deletions were unable to coimmunoprecipitate Myc-SINE1.

To further analyze SUN domain specificity of the protein–protein interactions, we introduced two point mutations in the SUN domain of AtSUN1 and AtSUN2. Based on the amino acid sequence alignment of AtSUN1, AtSUN2, and *Homo sapiens* SUN2 (Zhou and Meier, 2013), two conserved residues in the KASH-binding pocket were chosen and mutated in AtSUN1 (H439A and Y443F) and AtSUN2 (H434A and Y438F, illustrated in Fig. 3 B). The mutated proteins were named AtSUN1dMut and AtSUN2dMut, respectively. After *N. benthamiana* coexpression and co-IP, the ability of GFP-AtSUN1dMut and GFP-AtSUN2dMut to bind Myc-SINE1 or Myc-SINE2 was determined. As shown in Fig. 3 (F and G), in contrast to wild-type SUN proteins, both mutated proteins barely interacted with either SINE1 or SINE2, confirming that the KASH-binding pocket within the SUN domain is required for interaction.

Fig. 4 shows the comparable co-IP assays performed for GFP-tagged SINE3, SINE4, and SINE5 and their respective mutants, tested for interactions with Myc-tagged AtSUN1, AtSUN1dMut, AtSUN2, and AtSUN2dMut. IPs were performed with an anti-GFP antibody, and coimmunoprecipitated proteins were detected with an anti-Myc antibody. Fig. 4 A shows a schematic representation of SINE3, SINE4, SINE5, and their putative KASH domain mutants. Fig. 4 (B and C) shows that SINE3 strongly binds to AtSUN1 and AtSUN2 but that deletion

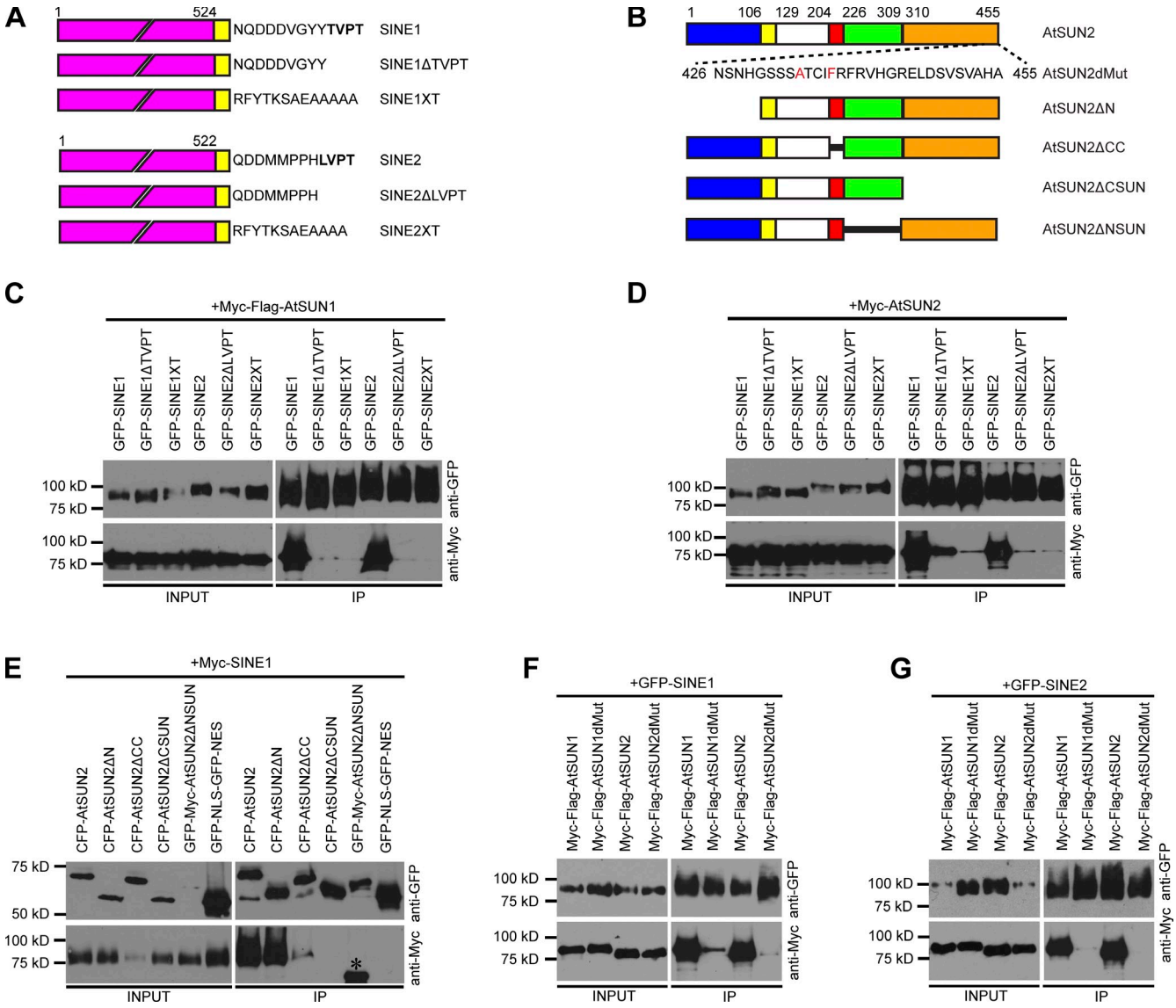

Figure 3. **Co-IP analysis of SINE1/2–AtSUN interactions.** (A) Domain organization of SINE1, SINE2, and their KASH domain mutants. The C-terminal 4 aa are indicated in bold. (B) Domain organization of AtSUN2 and its mutants. The C-terminal 30 aa of AtSUN2 are shown, and the residues changed in AtSUN2dMut are indicated in red. Diagrams in A and B were drawn to scale, with the gaps in A representing 300 aa. The numbers above each domain indicate the position of the first and the last amino acid of that domain. Magenta, domain N-terminal to the TMD of SINE1 or SINE2; blue, domain N-terminal to the TMD of AtSUN2; yellow, TMD; white, unknown domain; red, coiled-coil domain; green, N-terminal part of the SUN domain; orange, C-terminal part of the SUN domain. (C) SINE1 and SINE2 interact with AtSUN1 through their KASH domain. (D) SINE1 and SINE2 interact with AtSUN2 through their KASH domain. (E–G) AtSUN1 and AtSUN2 interact with SINE1 and SINE2 through their SUN domain. The asterisk in the bottom right of E indicates the codetected GFP-Myc-AtSUN2ΔNSUN band. In C–G, GFP-tagged proteins were immunoprecipitated and detected with anti-GFP antibodies. Myc-tagged proteins were detected with an anti-Myc antibody. The input/IP ratio is 1:9.

of the C-terminal 4 aa, replacement of the putative KASH domain, or mutating the KASH-binding pocket of AtSUN1 and AtSUN2 disrupts this binding. Similar results were obtained for SINE4 (Fig. 4, D and E) and for SINE5 (Fig. 4, F and G).

The NE localization of SINE1, SINE2, SINE3, SINE4, and SINE5 depends on AtSUN

Losing interaction with a SUN protein leads to mislocalization of Nesprin-2 (Padmakumar et al., 2005; Crisp et al., 2006), Nesprin-3 (Ketema et al., 2007), Nesprin-4 (Roux et al., 2009), KASH5 (Morimoto et al., 2012), and AtWIP1 (Zhou et al., 2012a). To determine whether this is true for GFP-SINE1ΔTVPT, GFP-SINE2ΔLVPT, GFP-SINE3ΔPLPT, GFP-SINE4ΔLVPT, and GFP-SINE5ΔLVPT, they were stably expressed in *A. thaliana* under the control of the 35S promoter. Fig. 2 B shows that all five GFP fusion proteins were only weakly associated with the nuclear periphery and were abundantly found in the cytoplasm and/or associated with the plasma membrane and components of the endomembrane system. This demonstrates that the C-terminal 4 aa are required for efficient association of all five proteins with the NE. To compare the NE localization quantitatively, we defined an NE localization index (NLI) as the sum of two maximum NE intensities divided by the sum of two maximum

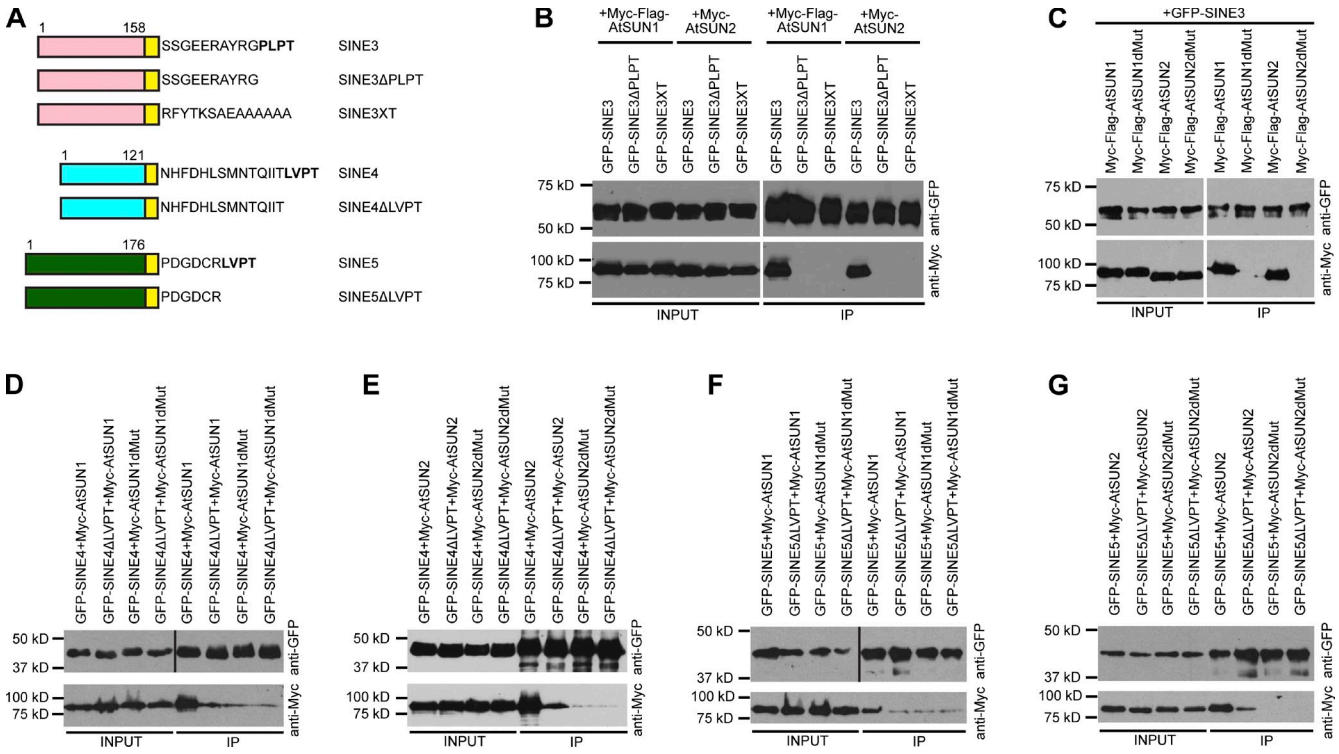

Figure 4. **Co-IP analysis of the SINE3/SINE4/SINE5–AtSUN interactions.** (A) Domain organization of SINE3, SINE4, SINE5, and their KASH domain mutants. Diagrams were drawn to scale. Pink, domain N-terminal to the TMD of SINE3; cyan, domain N-terminal to the TMD of SINE4; dark green, domain N-terminal to the TMD of SINE5; yellow, TMD. The numbers above each domain indicate the position of the first and the last amino acid of that domain. The C-terminal 4 aa are indicated in bold. (B) SINE3 interacts with AtSUN1 and AtSUN2 through its KASH domain. (C) AtSUN1 and AtSUN2 interact with SINE3 through their SUN domain. (D) SINE4 interacts with the SUN domain of AtSUN1 through its KASH domain. (E) SINE4 interacts with the SUN domain of AtSUN2 through its KASH domain. (F) SINE5 interacts with the SUN domain of AtSUN1 through its KASH domain. (G) SINE5 interacts with the SUN domain of AtSUN2 through its KASH domain. In B–G, GFP-tagged proteins were immunoprecipitated and detected with anti-GFP antibodies. Myc-tagged proteins were detected with an anti-Myc antibody. The input/IP ratio is 1:9. In D and F, the vertical black lines represent the removal of empty intervening lanes for presentation purposes.

cytoplasmic intensities ([N1 + N2]/[C1 + C2]; Fig. 2 D, top). The higher the NLI, the more concentrated at the NE the signal is. As shown in Fig. 2 D, deleting the C-terminal 4 aa of the SUN domain–interacting NE proteins (SINEs) significantly reduced their enrichment at the NE when compared with wild-type proteins (two-tailed *t* test, $P < 0.01$, $n = 30$).

Finally, GFP-tagged SINE1, SINE2, SINE3, SINE4, and SINE5 were expressed in a *sun1-knockout* (*KO*) *sun2-knockdown* (*KD*; *sun1-KO sun2-KD*) double mutant (Zhou et al., 2012a), respectively. Fig. 2 C shows that protein mislocalization similar to the deletion of the C-terminal 4 aa was also observed in the *sun1-KO sun2-KD* mutant, which is reflected by the NLI in Fig. 2 D.

AtSUN1 and AtSUN2 affect the mobility of SINE1 and SINE2 at the plant NE

Protein interactions will reduce the mobility of a membrane protein, and FRAP can assay this mobility difference (Reits and Neefjes, 2001). By expressing proteins in *N. benthamiana* leaves, the mobility at the NE of GFP-SINE1 and GFP-SINE2 with or without coexpression of AtSUN proteins was quantified by comparing maximum recovery values of FRAP. As shown in Fig. 5, the mobility of GFP-SINE1 and GFP-SINE2 was significantly reduced when they were coexpressed with either AtSUN1 or AtSUN2 (two-tailed *t* test, $P < 0.01$, $n = 35$). Coexpressing AtSUN1ΔNSUN with either SINE1 or SINE2 or coexpressing AtSUN2ΔNSUN with SINE2 had no effect, consistent with the finding that mutating the SUN domain disrupts binding in co-IP assays (two-tailed *t* test, $P > 0.05$, $n = 35$). A slight decrease in maximum recovery was detected when GFP-SINE1 was coexpressed with AtSUN2ΔNSUN (Fig. 5 B). It is possible that AtSUN2ΔNSUN retains some affinity for GFP-SINE1, which was not resolved by the co-IP assay (Fig. 3 E). Together, these data indicate that SINE1 and SINE2 interact with AtSUN1 and AtSUN2 at the plant NE.

SINE1 and SINE2 have different expression and localization patterns

No known domains are predicted in the newly confirmed KASH proteins by InterProScan, except for SINE1 and SINE2, which contain armadillo (ARM) repeats in their N termini. Because SINE1 and SINE2 are also the only known KASH proteins conserved across land plants, we investigated them in greater detail. To analyze the expression profiles of SINE1 and SINE2, we expressed N-terminally *GFP*-tagged *SINE1* and *SINE2* driven by their own promoter (*SINE1pro::GFP-SINE1* and *SINE2pro::GFP-SINE2*) in stably transformed wild-type *A. thaliana*. In leaves, confocal z-stack images show that *SINE1* was exclusively

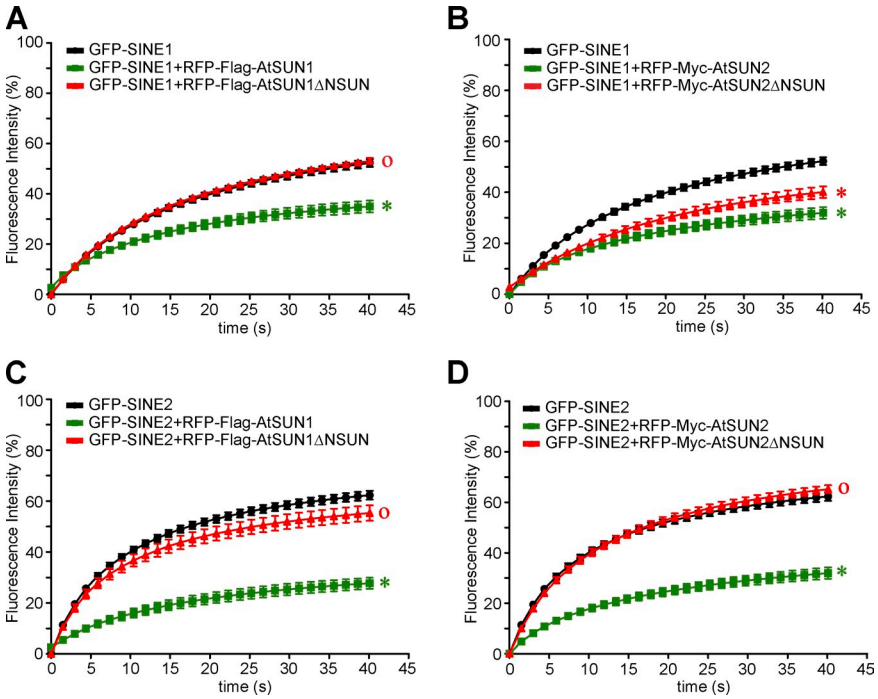

Figure 5. **FRAP analysis of the interaction between SINE1/2 and AtSUN.** Fluorescent protein fusions of SINE1, SINE2, and SUN proteins were transiently expressed in *N. benthamiana* leaves, and protein mobility was studied by FRAP. (A) Recovery curves of GFP-SINE1 alone or GFP-SINE1 coexpressed with RFP-Flag-AtSUN1 or RFP-Flag-AtSUN1ΔNSUN, respectively. (B) Recovery curves of GFP-SINE1 alone or GFP-SINE1 coexpressed with RFP-Myc-AtSUN2 or RFP-Myc-AtSUN2ΔNSUN, respectively. (C) Recovery curves of GFP-SINE2 alone or GFP-SINE2 coexpressed with RFP-Flag-AtSUN1 or RFP-Flag-AtSUN1ΔNSUN, respectively. (D) Recovery curves of GFP-SINE2 alone or GFP-SINE2 coexpressed with RFP-Myc-AtSUN2 or RFP-Myc-AtSUN2ΔNSUN, respectively. Color-coded asterisks after each curve indicate that the maximum recovery of that curve shows a statistically significant difference when compared with the black curve ($P < 0.01$, two-tailed *t* test, $n = 35$), whereas color-coded circles after each curve indicate no statistical significant difference ($P > 0.05$, two-tailed *t* test, $n = 35$). Error bars represent SEMs.

expressed in guard cells and guard cell mother cells (Fig. 6 A, Fig. 7 A, and Fig. S3 A), whereas *SINE2* was expressed in epidermal cells, mesophyll cells, and trichomes but only weakly in guard cells (Fig. 6 B, Fig. 7 B, and Fig. S3 A). Both *SINE1* and *SINE2* are expressed in roots, without any obvious differences (Fig. 7). These expression patterns were also recapitulated in *A. thaliana* lines transformed with *SINE1pro::GFP–β-glucuronidase* (*GUS*) or *SINE2pro::GFP-GUS* (Fig. S3 B, three lines of each construct were analyzed, and representative images are shown).

Interestingly, GFP-SINE1 labeled a spotted, fiberlike pattern at the NE and in the cytoplasm of guard cells and guard cell mother cells (Fig. 6 A and Fig. S4 A). In root cells, the fiberlike pattern was more prominent at the NE (Fig. 7 A). However, SINE2 showed no fiberlike localization pattern in either leaves or roots (Fig. 6 B and Fig. 7 B).

SINE1 is associated with F-actin through its ARM repeats

Because ARM repeats are predicted in the N termini of SINE1 and SINE2 (aa 3–286 and aa 17–289, respectively), the N-terminal 308 aa of SINE1 and the N-terminal 309 aa of SINE2 were fused to GFP (GFP-SINE1$^{1–308}$ and GFP-SINE2$^{1–309}$, respectively) and transiently expressed in *N. benthamiana* leaves under the control of the 35S promoter. GFP-SINE1$^{1–308}$ was localized to cytoplasmic fiberlike structures. We then coexpressed GFP-SINE1$^{1–308}$ with an F-actin marker, RFP-Lifeact (Riedl et al., 2008), or a microtubule marker, MAP4-RFP, in *N. benthamiana* leaves. As shown in Fig. 8 A, GFP-SINE1$^{1–308}$ was colocalized with RFP-Lifeact but not with MAP4-RFP. The colocalization of GFP-SINE1$^{1–308}$ with RFP-Lifeact was also observed in root cells of stably transformed *A. thaliana* (Fig. 8 B). In contrast, GFP-SINE2$^{1–309}$ did not decorate fiberlike structures in *N. benthamiana* leaves (Fig. 8 A) and neither did the fusion of a larger N-terminal fragment, excluding the TMD-KASH domain (SINE2$^{1–521}$; Fig. S4 B). Both GFP-SINE2$^{1–309}$ and GFP-SINE2$^{1–521}$ had similar localization to the soluble protein GFP-NLS-GFP-NES (Fig. S4 B). This suggests that SINE1 associates with F-actin and that this property is not shared with SINE2.

Because the ARM repeats of SINE1 are associated with F-actin, we reasoned that the NE fibers decorated by GFP-SINE1 (Fig. 6 A, Fig. 7 A, and Fig. S4 A) are likely associated with and/or depend on F-actin. Rhodamine-phalloidin (an F-actin binding dye) staining of the guard cells expressing *GFP-SINE1* showed that GFP-SINE1 was colocalized with rhodamine-phalloidin–labeled fibers (Fig. 9 A). After treatment with 10 µM Latrunculin B (LatB) for 1 h, the SINE1 NE fibers disappeared (Fig. 9 B). In contrast, in the mock treatments, the NE fibers were barely affected (Fig. 9 B). Next, we investigated whether the mobility of SINE1 and SINE2 at the NE was affected by actin depolymerization. As measured by FRAP, 25 µM LatB treatment increased the mobility of GFP-SINE1 (two-tailed *t* test, $P < 0.01$, $n = 35$; Fig. 9 C) in guard cells but had no effect on the mobility of GFP-SINE2 (two-tailed *t* test, $P > 0.05$, $n = 35$; Fig. S4 C), consistent with a specific interaction between SINE1 and F-actin at the guard cell NE.

SINE1 is required for proper nuclear anchorage in guard cells

To probe into the biological roles of *SINE1* and *SINE2*, three *SINE1* transfer DNA (T-DNA) insertion mutants (*sine1-1*, *sine1-2*, and *sine1-3*) and two *SINE2* T-DNA insertion mutants (*sine2-1* and *sine2-2*) were isolated. Further analysis showed that at least one downstream gene is missing in *sine1-2*, which was therefore discarded. *sine2-1* carries the homozygous *qrt1-2* allele (Francis et al., 2006), which was removed by segregation in the *sine1-1 sine2-1* double mutant. All T-DNA insertion

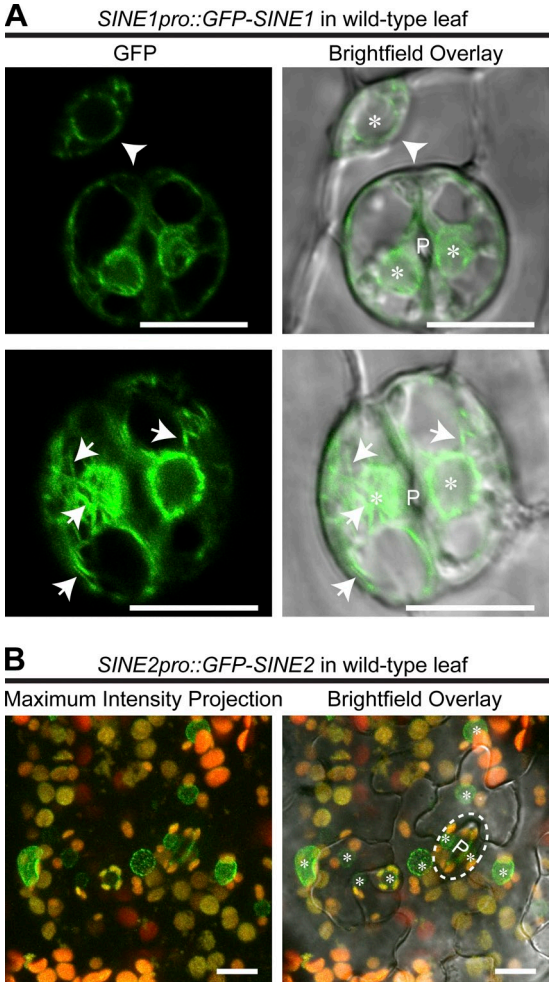

Figure 6. **Expression and protein localization pattern of SINE1 and SINE2 in leaves.** (A) *SINE1* is expressed in guard cells and guard cell mother cells (top, arrowheads), and the protein is localized to fibers in guard cells (bottom, arrows). (B) *SINE2* is expressed mainly in epidermal cells and mesophyll cells and weakly in guard cells (circled by a dotted ellipse). The images are maximum intensity projections of a z-stack image. Autofluorescence of chloroplasts are shown in red and overlaid with the GFP signal. Bars, 10 µm. In the overlay images, asterisks indicate the nuclei observed, and P letters indicate stomatal pores enclosed by pairs of guard cells.

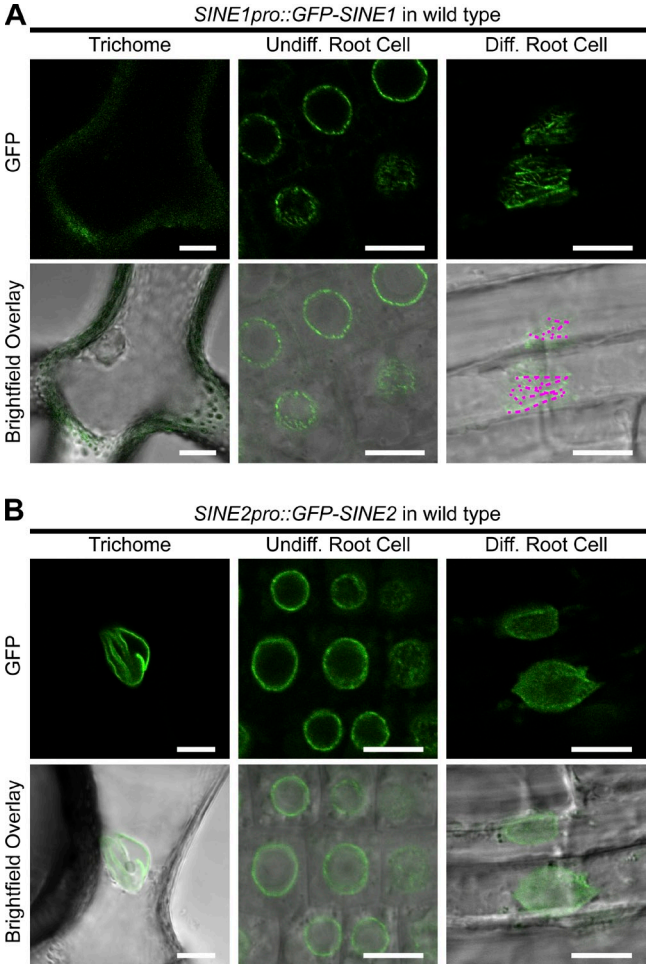

Figure 7. **Expression and protein localization pattern of SINE1 and SINE2 in trichomes and roots.** (A) Expression and protein localization pattern of *SINE1* in trichomes and roots. (B) Expression and protein localization pattern of *SINE2* in trichomes and roots. Both genes are expressed in root cells, but only *SINE2* is expressed in trichomes. Both proteins are localized at the NE. The trichome image of GFP-SINE1 was taken with 5× higher laser power (50%) than that used for GFP-SINE2, as indicated by the autofluorescence from the trichome cell wall. For the differentiated root cells, the nuclear surface was imaged to compare the fiber structure of GFP-SINE1 (outlined by dotted magenta lines in the overlay image) and relatively evenly distributed signal of GFP-SINE2. Bars, 10 µm. Diff., differentiated; Undiff., undifferentiated.

sites were confirmed by sequencing and are illustrated in Fig. 10 A. RT-PCR shows that no full-length *SINE1* mRNA accumulates in *sine1-1* and *sine1-3* and no full-length *SINE2* mRNA accumulates in *sine2-1* and *sine2-2* (Fig. 10 B). All mutant lines (*sine1-1*, *sine1-3*, *sine2-1*, and *sine2-2* single mutants and *sine1-1 sine2-1*, *sine1-1 sine2-2*, and *sine1-3 sine2-2* double mutants) appeared phenotypically normal under standard laboratory conditions.

Because *SINE1* is predominantly expressed in guard cells, we examined guard cell nuclear positioning. The leaf epidermis was peeled and immediately fixed in 4% paraformaldehyde containing 4 µM Hoechst 33342. An ellipse was rendered on a pair of guard cells, and the acute angle between the minor axis of the ellipse to the center of the nucleus was used to quantify the position of the nucleus (Fig. 10 C). Only guard cell pairs with a major axis of the rendered ellipse longer than 8 µm were measured. To avoid stomatal aperture effects on nuclear position, we irradiated the leaves with 100 µmol/m^2/s blue light to open stomata before fixation. 86 pairs of guard cells were measured for each line. In wild type, the guard cell nuclei predominantly localized at the center of each cell, and this positioning was not affected in *sine2-2* (Fig. 10 D, two-tailed *t* test, $P > 0.05$, $n = 172$). However, in mutants containing homozygous *sine1-1* or *sine1-3* alleles, the position of the nuclei skewed toward a greater distance from the center of a guard cell (two-tailed *t* test, $P < 0.01$, $n = 172$; Fig. 10 D). We then measured the nuclear position without blue light illumination. As shown in Fig. 10 D, similar results were obtained, suggesting that stomatal aperture has little effect on nuclear positioning in guard cells. Guard cell nuclear position was also affected in *sun1-KO sun2-KD* (compared with wild type, two-tailed *t* test, $P < 0.01$, $n = 172$) and was similar to that of *sine1-1* (two-tailed *t* test, $P > 0.05$, $n = 172$).

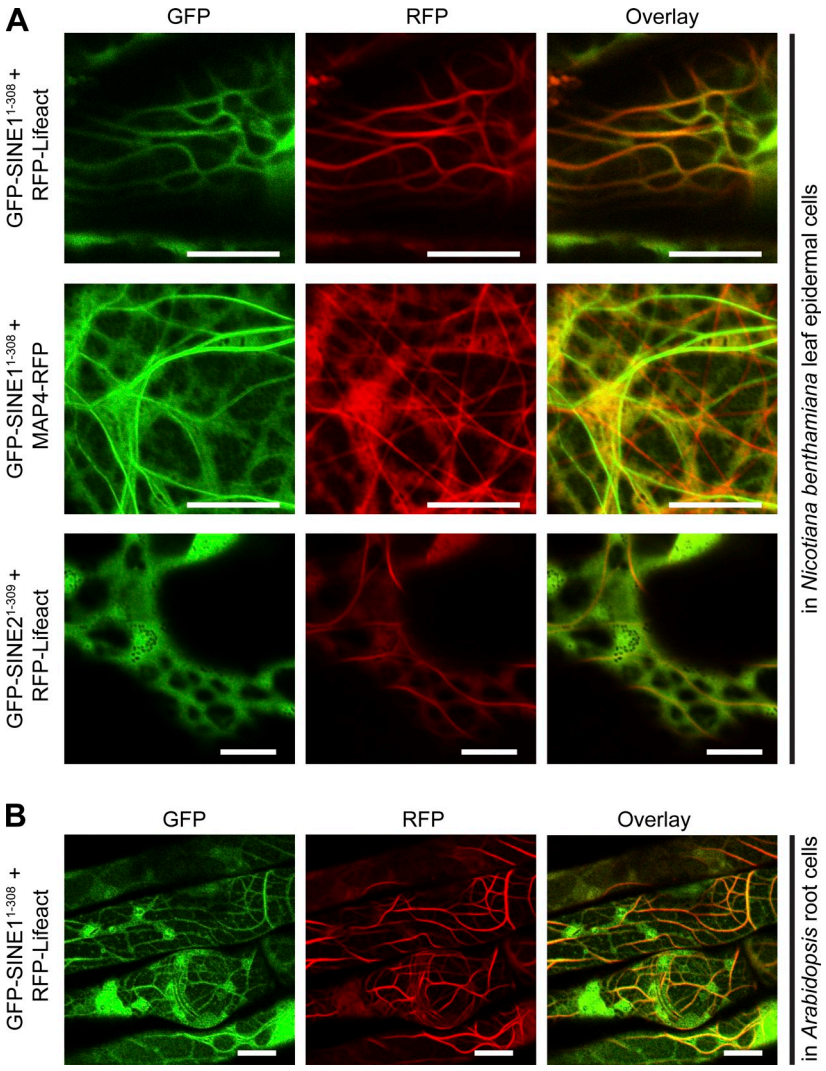

Figure 8. **Association of SINE1$^{1–308}$ with F-actin filaments.** (A) GFP-SINE1$^{1–308}$ was transiently coexpressed with RFP-Lifeact (first row) or MAP4-RFP (middle row) in *N. benthamiana* leaves, showing that GFP-SINE1$^{1–308}$ was colocalized with RFP-Lifeact but not MAP4-RFP. GFP-SINE2$^{1–309}$ was transiently coexpressed with RFP-Lifeact in *N. benthamiana* leaves (bottom row), but GFP-SINE2$^{1–309}$ was localized to the cytoplasm instead of F-actin fibers labeled by RFP-Lifeact. (B) GFP-SINE1$^{1–308}$ and RFP-Lifeact were colocalized in root cells of stably transformed *A. thaliana* plants. Bars, 10 µm.

Next, we measured the guard cell nuclear position in *sine1-1* complemented by *SINE1pro::GFP-SINE1*. Three lines were analyzed, and in all cases, *SINE1pro::GFP-SINE1* rescued the nuclear position of *sine1-1*, as shown in Fig. 10 D (compared with wild type, $P > 0.05$; compared with *sine1-1*, $P < 0.01$; two-tailed *t* test; $n = 172$). Importantly, 10 µM LatB treatment also affected guard cell nuclear position and recapitulated the *sine1-1* effect (compared with wild type or line 3, two-tailed *t* test, $P < 0.01$, $n = 172$; Fig. 10 D). Mock treatment showed no effect (compared with wild type or line 3, two-tailed *t* test, $P > 0.05$, $n = 172$; Fig. 10 D). These data strongly suggest that the AtSUN–SINE1 complex is involved in centrally anchoring the paired guard cell nuclei in an F-actin–dependent manner, likely by direct or indirect interaction of the SINE1 ARM repeats with F-actin.

SINE2 contributes to *A. thaliana* innate immunity to an oomycete pathogen

Upon contact with plant cells, filamentous plant pathogens develop haustoria, sophisticated feeding structures that form a specific membrane interface with the host cell. Haustorium formation leads to structural rearrangements in the attacked host cell, and this involves migration of the nucleus toward the infection site (Gross et al., 1993; Skalamera and Heath, 1998; Schmelzer, 2002; Caillaud et al., 2012; Graumann and Evans, 2013). To suppress plant immunity, pathogens translocate effector proteins into host cells, several of which are targeted to the host cell nucleus (Deslandes and Rivas, 2011). We therefore tested whether immunity to the *A. thaliana* downy mildew pathogen *Hyaloperonospora arabidopsidis* (*Hpa*) is altered in *SINE1* and *SINE2* mutants. 10-d-old seedlings were infected with *Hpa* isolate Noco2 that infects Col-0, and the severity of the infection was quantified by counting the conidiophores that emerged from the upper side of the cotyledons 6 d after infection. As shown in Fig. 10 E, *sine2-2*, *sine1-1 sine2-1*, and *sine1-1 sine2-2* were more susceptible to *Hpa* Noco2 than wild type, but *sine1-1* behaved like wild type (one-way analysis of variance $\alpha < 0.01$ followed by Tukey's honest significant difference test $\alpha < 0.01$, $n = 120$). Expression of *SINE2pro::GFP-SINE2* in the *sine1-1 sine2-1* double mutant complemented the enhanced disease susceptibility phenotype in two independent transgenic lines (Fig. 10 E). These results suggest that *SINE2*, but not *SINE1*, contributes significantly to plant immunity against *Hpa*.

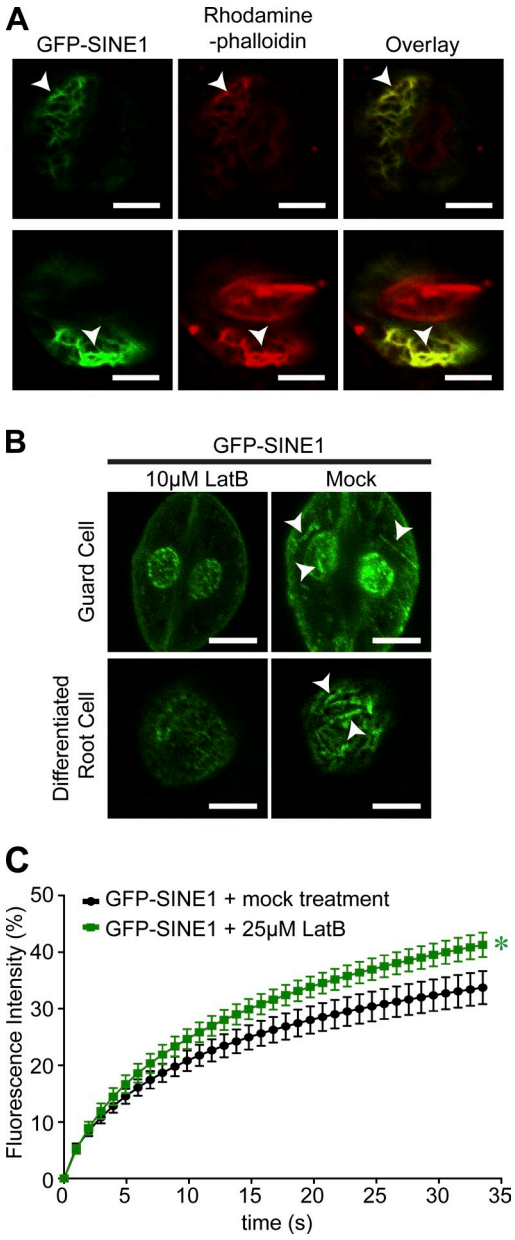

Figure 9. **Association of SINE1 with F-actin filaments in guard cells.** (A) GFP-SINE1 is colocalized with rhodamine-phalloidin–labeled filaments in *A. thaliana* guard cells (arrowheads). (B) The SINE1 fibers in both guard cells and root cells are sensitive to 1-h treatment of 10 µM LatB, but the fibers (arrowheads) are still visible in the mock treatment. The images of guard cells are maximum intensity projections of a z-stack image. The differentiated root cell nuclei were imaged at the nuclear surface. (C) FRAP recovery curves of GFP-SINE1 with or without LatB-triggered F-actin depolymerization. *A. thaliana* lines stably transformed with GFP-SINE1 driven by the 35S promoter were used for FRAP. The asterisk indicates a significant statistical difference of the maximum recovery compared with the black curve (two-tailed *t* test, $P < 0.01$, $n = 35$). Error bars represent SEMs. Bars, 5 µm.

Discussion

DORY as a useful tool to identify potential KASH proteins

In this study, the algorithm DORY was developed, which predicted 10 new plant KASH protein families. Five members from four predicted families were verified to be bona fide plant KASH proteins. The success suggested that DORY had robust and efficacious predictive power. Using the C-terminal amino acid pattern PPPX and the nr database, DORY predicted animal coiled-coil domain–containing protein 155 (Ccdc155) and lymphoid-restricted membrane protein (Lrmp) as potential KASH proteins. Ccdc155 was recently published as KASH5 (Morimoto et al., 2012; Horn et al., 2013), and Lrmp was also identified as a KASH protein homologous to Ccdc155 (Lindeman and Pelegri, 2012; Horn et al., 2013). Thus, we used DORY to deep search for unrecognized animal KASH proteins. Homologues of known animal KASH proteins were obtained by BLASTP, and the C-terminal 4-aa pattern [PATHQL]PP[QTVFILM] was used for searching for animal KASH proteins in the nr database using DORY with the maximum KASH domain length set to 60. Five new potential KASH proteins were identified. Their C termini were aligned with the C termini of T191C and known animal KASH proteins (Fig. S2 G). *Loa loa* GI312089182, *Wuchereria bancrofti* GI402593023, and *Brugia malayi* GI170594686 are homologues and can only be found in these filarial nematodes. *Branchiostoma floridae* GI260805382 is species specific. This information might serve as a starting point for experimental investigation to researchers in the respective fields.

Diversity of KASH proteins

The SUN domain is well conserved among eukaryotes (Starr and Fridolfsson, 2010). AtSUN1dMut and AtSUN2dMut point mutations were informed by the corresponding KASH-binding pocket of mammalian SUN2 and abolish plant KASH-binding ability (Fig. 3 and Fig. 4). This indicates that the plant SUN domain and mammalian SUN domain share both sequence and structural similarities. In contrast, there is little to no sequence similarity between the plant KASH domains and opisthokont KASH domains. The plant KASH domains are much shorter (~9–16 aa) than those of most opisthokont KASH proteins (~30 aa). However, the crystal structure of the SUN trimer indicated that the length of the entire luminal domain of *H. sapiens* SUN2 was predicted to span the NE lumen (Sosa et al., 2012), indicating that this may be also the case for plant SUN proteins, and the shorter plant KASH domains should be sufficient to reach the SUN domain.

The plant KASH protein families revealed here differ vastly in terms of their conservation within the land plant lineage. SINE1 and SINE2 are conserved across land plants, including nonvascular plants. This suggests an ancient appearance and makes SINE1/2 family members exciting candidates to probe into an early, conserved function of plant NE bridging complexes. In contrast, WIP is conserved in flowering plants, whereas SINE3 and its homologues are only found in dicots, indicating a much later appearance of these SUN-binding partners. Other proteins, including the SINE4 family and the SINE5 family, are present in only a few closely related species, suggesting rather specific functions.

A similar pattern can be derived by comparing prevalence among opisthokont KASH proteins. Homologues of ANC-1, MSP-300, Nesprin-1, and Nesprin-2 are widely conserved in animals (Starr and Fridolfsson, 2010), Klarsicht homologues can only be found in insects (our BLASTP search, proteins with

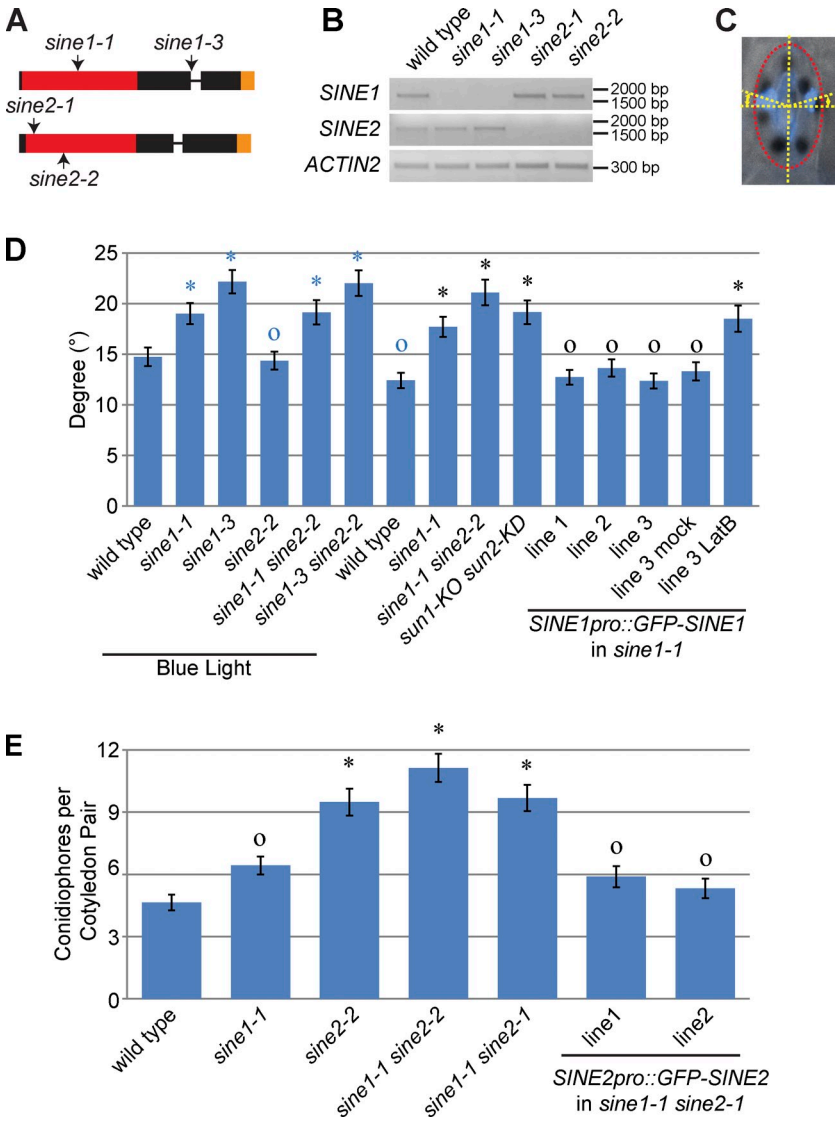

Figure 10. **Biological roles of SINE1 and SINE2.** (A) T-DNA insertion sites of *sine1-1*, *sine1-3*, *sine2-1*, and *sine2-2*. The left borders of T-DNA insertion sites were confirmed by sequencing and indicated by arrows on *SINE1* and *SINE2* genomic structures (drawn to scale). Exons are depicted as filled bars, and introns are depicted as lines. DNA fragments encoding the ARM repeats and the TMD-KASH domain are shown in red and orange, respectively. (B) RT-PCR determination of the expression levels of *SINE1* and *SINE2* in their mutants. Primers amplified the full-length coding sequences are listed in Table S2. (C) Example of measuring nuclear position in guard cells. An ellipse was rendered on a pair of guard cells, and the acute angle between the center of the nucleus and the minor axis (indicated by curved double-headed arrows) was measured. (D) Mean guard cell nuclear positions determined by the angle shown in C. Blue asterisks, $P < 0.01$ when compared with wild type after blue light treatment; blue circles, $P > 0.05$ when compared with wild type after blue light treatment; black asterisks, $P < 0.01$ when compared with wild type without blue light treatment; black circles, $P > 0.05$ when compared with wild type without blue light treatment. Two-tailed *t* test was used and $n = 172$. (E) Quantification of conidiophore formation on the cotyledon adaxial side as a measure of *Hpa* Noco2 growth on the indicated genotypes. Values are means ± SE of three biological replicates, each with $n = 40$. Asterisks indicate significant differences to wild type, and circles represent no significant differences to wild type. One-way analysis of variance ($\alpha < 0.01$; $n = 120$) followed by Tukey's honest significant difference test ($\alpha < 0.01$) was used.

an E-value < 0.0001 were considered as homologues), and KDP-1 homologues are specific to several nematodes (McGee et al., 2009). No close homologues of *Schizosaccharomyces pombe* Kms1 and Kms2 can be found in other species (our BLASTP search, proteins with E-value < 0.0001 were considered as homologues). This cross kingdom and within kingdom differentiations of KASH proteins imply that they have emerged after the rise of SUN proteins and that they evolved rapidly to accommodate various functionalities. Given the diverse sequences of the N-terminal domains of plant KASH proteins, detailed future studies will be required to understand their functions in the land plant lineage.

The LINC function of plant SUN-KASH NE bridges

Plant SUN-WIP NE bridges were recently linked to the actin cytoskeleton. AtWIT1 (*A. thaliana* WIT1) and AtWIT2 interact with AtWIP1/2/3 and recruit myosin XI-I to the NE (Tamura et al., 2013). Loss of myosin XI-I or AtWIT1/2 leads to restricted nuclear movement and altered nuclear morphology in root and leaf cells. The F-actin association and nuclear positioning role of SINE1 that were identified here provide another example of plant LINC complexes. Transmembrane actin-associated nuclear (TAN) lines formed by SUN2 and Nesprin-2 were found in mammalian fibroblasts (Luxton et al., 2010). TAN lines transfer forces from F-actin to the nucleus, mediating the backward movement of the nucleus during fibroblast polarization (Luxton et al., 2010). However, unlike the parallel TAN lines, SINE1 NE fibers are interwoven (Fig. 6), which might relate to their function in nuclear anchorage.

Why the guard cell nuclei are positioned in a paired, central location is not known, but it is noteworthy that SINE1 fibers are extended from the NE to the cytoplasm in guard cells (Fig. 6 A and Fig. S4 A). F-actin rearrangement has been found to be essential for stomata opening or closing. These processes are retarded when F-actin filaments are stabilized either by using F-actin binding reagents or by mutations in actin-related protein 2/3 complex (Eun and Lee, 1997; MacRobbie and Kurup, 2007; Higaki et al., 2010; Jiang et al., 2012; Li et al., 2013). Therefore, it is conceivable that SINE1 fibers may sense the F-actin rearrangement,

transmit the signal to the nucleus, and trigger downstream gene regulatory events. This testable hypothesis can form the foundation for future investigations into the unexplored nuclear biology of plant guard cells.

Differentiated expression patterns and functions of SINE1 and SINE2

Already, the dissection of the SINE1/2 family revealed a divergence of both function and expression pattern. This is reminiscent of mammalian NETs, whose expressions differ notably in different tissues and which perform tissue-specific functions (Korfali et al., 2012; de las Heras et al., 2013). SINE1, predominantly expressed in guard cells, forms F-actin–associated fibers through its ARM repeats and is involved in the central positioning of the paired guard cell nuclei. Although the ARM repeats are conserved in SINE2, SINE2 does not form F-actin–associated structures and is not involved in positioning the guard cell nuclei. Instead, a KO of *SINE2* attenuates *A. thaliana* immunity to the oomycete pathogen *Hpa*. This function correlates well with its expression pattern—predominantly expressed in leaf epidermal and mesophyll cells in leaves—because oomycete hyphae usually invade plants through the junction of two epidermal cells and insert haustoria into the epidermal and mesophyll cells during its subsequent growth (Guest, 1986; Coates and Beynon, 2010). SINE2's specific contribution to resistance will require further dissection. Nonetheless, our current data already show a clear functional divergence within the SINE1/2 family and will be highly informative for choosing individual SINE1/2 family candidates from crop species for further investigation.

In summary, this study dramatically expands our knowledge of plant NETs and delivers an effective tool for identifying KASH proteins. The functional study of the SINE1/2 family already suggests that members in the same, evolutionarily old KASH protein family have diverged into playing separate, important roles in plant biology. This implies that the detailed study of many more of the newly identified KASH proteins by reverse genetic methods has the potential to reveal numerous unrecognized processes in plant cell and specifically plant nuclear biology. Our findings support the hypothesis of an independent evolution of SUN-dependent NE bridges after the opisthokont–plant separation. The lack of similarity between the identified plant KASH proteins and the known opisthokont KASH proteins suggests that plants have recruited, during evolution, a different set of membrane proteins at the outer NE.

Materials and methods

KASH candidate in silico search

Please refer to Fig. S1 B for details of DORY and Supplemental material. The TAIR10 protein models were downloaded from TAIR (The Arabidopsis Information Resource). The nr database is constantly updated, which affects the results of our program and NCBI BLASTP. The one used here was downloaded on February 19, 2013.

To develop the C-terminal 4-aa pattern of plant KASH proteins, we searched the *A. thaliana* TAIR10 protein models using our program with pattern XXPT (X represents any amino acid). Five protein models were identified: At1G54385.1, At3G03970.1, At3G06600.1, At4G24950.1, and At3G47410.1. Homologues of newly identified plant KASH candidates were obtained using NCBI BLASTP on June 3, 2013 (proteins with E value < 0.0001 were considered homologues), and the TMD prediction program Phobius (http://phobius.sbc.su.se/; Käll et al., 2007) was used to support the existence of a TMD. For convenience, the GenInfo Identifier (GI) number is used to represent the corresponding protein in this study. If the majority of a protein family terminates in a putative KASH domain, this protein family was considered a positive candidate. Among the five protein models identified, At1G54385.1 (SINE1), At3G03970.1 (SINE2), At3G06600.1 (SINE3), and At4G24950.1 (SINE4) were positive candidates (Fig. 1 A). At3G47410.1 has one homologue in *A. thaliana*, two in *A. lyrata*, and one in *C. rubella*. Two *A. thaliana* homologues do not possess a putative KASH domain. It was therefore considered a false positive.

Analyzing the C-terminal 4 aa of homologues of WIP1/2/3, SINE1/2, SINE3, and SINE4 revealed a new pattern of [DTVAMPLIFY][VAPIL]PT (brackets indicate alternative amino acid residues at the respective position). This pattern was used to search the nr database for putative KASH proteins in plants using DORY.

We performed BLASTP using the protein sequence of SINE1 and SINE2 (which are conserved across land plants) against individual nonplant organisms, such as *H. sapiens*, *Mus musculus*, *Caenorhabditis elegans*, *Drosophila melanogaster*, *S. pombe*, and *Saccharomyces cerevisiae*, and no homologues were found. We also performed BLASTN using genomic sequence of *SINE1*, *SINE2*, *SINE3*, and *SINE4* and *SINE5* against nonplant genomes and obtained no hits. These results suggest that all SINEs are indeed plant specific, and they could not have been identified by homologous searches, such as BLASTN or BLASTP.

For the animal KASH protein search, homologues of known animal KASH proteins—Nesprin-1, Nesprin-3, Nesprin-4, Klarsicht, UNC-83, KASH5, and Lrmp—were obtained by BLASTP. Sequences containing no proline in the C-terminal 4 aa were submitted to BLASTP and removed if the closest homologue was not a KASH protein. The C-terminal 4-aa pattern [PATHQL]PP[QTVFILM], or very rarely PLPV, PSPT, or PPKA, was derived from the final KASH protein pool. Pattern [PATHQL]PP[QTVFILM] was used to search for putative animal KASH proteins. All alignments were performed by using MAFFT (Katoh and Standley, 2013) with default settings and the E-INS-i strategy, except for the alignment in Fig. S2 G, for which the G-INS-i strategy was used.

Protein model correction based on the TMD-putative KASH domain architecture

While searching for homologues of newly identified putative KASH proteins, we found many proteins share high similarities at the N termini but lack a putative KASH domain. Some of these cases were a result of a probably mispredicted intron and were then corrected based on the TMD-putative KASH domain architecture. Correction of *Selaginella moellendorffii* GI302806946 is supported by EST GI169026300. Correction of *Glycine max* GI356508173 is supported by EST GI21889745 and GI6847292. Correction of *G. max* GI356510247 is supported by EST GI7796284. Correction of *Vitis vinifera* GI147788255 is supported by EST GI30321072, GI110420183, and GI33406362. The corrected protein sequences are available as a dataset in Supplemental material.

Plant materials

A. thaliana (Columbia ecotype) were grown at 25°C in soil under 16-h light and 8-h dark or on Murashige and Skoog (Caisson Laboratories) medium with 1% sucrose under constant light. Ecotype Col-0 was used as wild type. The *sun1-KO sun2-KD* mutant was a gift from S. Armstrong and K. Osman (University of Birmingham, Birmingham, England, UK) and has been reported previously (Zhou et al., 2012a). *sun1-KO* (SALK_123093) is in Col-0 background with the T-DNA inserted in the first intron. *sun2-KD* (SALK_049398) is in Col-0 background with the T-DNA inserted in the 3′ UTR. *N. benthamiana* plants were grown at 28°C in soil under constant light. *sine1-1* (SALK_018239C), *sine1-2* (SALK_143274), *sine2-1* (CS801355), and *sine2-2* (CS1006876) were obtained from the Arabidopsis Biological Resource Center. *sine1-3* (GK-485E08-019738) was obtained from GABI-Kat. The primers used for genotyping are listed in Table S2. Genotyping of the *qrt1-2* allele in *sine2-1* was performed as reported by Francis et al. (2006).

Constructs

CFP-AtSUN2, *CFP-AtSUN2ΔN*, *CFP-AtSUN2ΔCC*, and *CFP-AtSUN2ΔCSUN* were described by Graumann et al. (2010). In brief, coding sequences of *AtSUN2*, *AtSUN2ΔN*, *AtSUN2ΔCC*, and *AtSUN2ΔCSUN* were amplified by PCR and cloned into the pDONR207 vector. After confirmation by sequencing, they were moved to pB7WGC2 (Karimi et al., 2002) by LR reaction (Invitrogen) to obtain the CFP-fused constructs. *Myc-Flag-AtSUN1*, *Myc-AtSUN2*, *GFP-Myc-AtSUN2ΔNSUN*, *RFP-Flag-AtSUN1*,

RFP-Flag-AtSUN1ΔNSUN, *RFP-Myc-AtSUN2*, and *RFP-Myc-AtSUN2ΔNSUN* were described previously (Zhou et al., 2012a). In brief, coding sequences of *Flag-AtSUN1*, *Myc-AtSUN2*, *Flag-AtSUN1ΔNSUN*, and *Myc-AtSUN2ΔNSUN* were amplified by overlap extension PCR and were cloned into the pENTR/D-TOPO (Invitrogen) vector. After sequencing, the coding sequences were moved from pENTR/D-TOPO to destination vectors by LR reaction. *Flag-AtSUN1* and *Myc-AtSUN2* were moved to pGWB21 (Nakagawa et al., 2007) to obtain *Myc-Flag-AtSUN1* and *Myc-AtSUN2*. *Myc-AtSUN2ΔNSUN* was moved to pK7WGF2 (Karimi et al., 2002) to obtain *GFP-Myc-AtSUN2ΔNSUN*. *Flag-AtSUN1*, *Flag-AtSUN1ΔNSUN*, *Myc-AtSUN2*, and *Myc-AtSUN2ΔNSUN* were moved to pK7WGR2 (Karimi et al., 2002) to obtain the RFP-fused constructs. PCR-based cloning was used to generate the other constructs, and the primers used are listed in Table S1. In brief, *Lifeact* was amplified by PCR using a self-annealing primer pair without templates and cloned to pENTR/D-TOPO. RT-PCR was used to amplify *SINE1*, *SINE2*, *SINE3*, and *SINE5* from cDNA. *SINE4* was amplified directly from wild-type genomic DNA by PCR. *NLS-GFP-NES* was amplified by overlapping PCR using vector pK7WGF2 as a template. All PCR products were cloned into the pENTR/D-TOPO vector and confirmed by sequencing. These clones were then used as templates for amplifying *SINE1ΔTVPT*, *SINE1XT*, *SINE1*$^{1–308}$, *SINE2ΔLVPT*, *SINE2XT*, *SINE2*$^{1–309}$, *SINE2ΔKASH*, *SINE3ΔPLPT*, *SINE3XT*, *SINE4ΔLVPT*, and *SINE5ΔLVPT* by PCR. PCR products were cloned into pENTR/D-TOPO vector and confirmed by sequencing. The coding sequences cloned into pENTR/D-TOPO were moved to destination vectors described by Karimi et al. (2002) by LR reaction (Invitrogen) to obtain N-terminal GFP-tagged protein constructs: *Lifeact* was cloned into pH7WGR2; *SINE1*, *SINE1ΔTVPT*, *SINE1XT*, *SINE1*$^{1–308}$, *SINE2*, *SINE2ΔLVPT*, *SINE2XT*, *SINE2*$^{1–309}$, *SINE2ΔKASH*, *SINE3ΔPLPT*, *SINE3XT*, *SINE4*, *SINE4ΔLVPT*, *SINE5ΔLVPT*, and *NLS-GFP-NES* were cloned into pK7WGF2; and *SINE3* and *SINE5* were cloned into pH7WGF2. *Flag-AtSUN1dMut* and *Myc-AtSUN2dMut* were obtained using the site-directed mutagenesis kit (QuikChange; Agilent Technologies), and the pENTR/D-TOPO vector containing the *Flag-AtSUN1* or the *Myc-AtSUN2* coding sequences described by Zhou et al. (2012a) was used as a template. After sequencing, *Flag-AtSUN1dMut* and *Myc-AtSUN2dMut* were cloned into pGWB21 to obtain *Myc-Flag-AtSUN1dMut* and *Myc-AtSUN2dMut*, respectively.

The hygromycin B resistance cassette was amplified by PCR from the vector pH2GW7 (Karimi et al., 2002) using 5′-AATGAATTCATCAGCTTGCATGCCGGTCGATC-3′ and 5′-GCTGAATTCATCATACATGAGAATTAAGGGAGTC-3′ (the EcoRI site is underlined), digested by EcoRI, and then ligated with the EcoRI-digested binary vector pPZP-RCS2 (Goderis et al., 2002). After confirmation by sequencing, the pPZP-RCS2-Hyg vector was obtained. The GFP-Gateway-35ST (35S terminator of Cauliflower Mosaic Virus) cassette was amplified by PCR using 5′-TATGGCGCGC[CACGTG]AGCAAGGGCGAGGAGCTGTTC-3′ (the AscI site is underlined, and the PmlI site is shown in brackets) and 5′-CCGGGGATCCTCTAGAGGGCC-3′ (the XbaI site is underlined), digested by AscI and XbaI, and ligated with the AscI–XbaI-digested pPZP-RCS2-Hyg. After confirmation by sequencing, the pHOAG vector was obtained.

SINE1 and *SINE2* promoters were amplified from *A. thaliana* genomic DNA (~2 kb; primers used are listed in Table S1), digested with AscI, and linked to the AscI–PmlI-digested pHOAG to obtain pHSINE1proAG and pHSINE2proAG, respectively. By LR reaction, the *SINE1* coding sequence was moved from the pENTR/D-TOPO to pHSINE1proAG to obtain the *SINE1pro::GFP-SINE1* construct, and the *SINE2* coding sequence was moved from the pENTR/D-TOPO to pHSINE2proAG to obtain the *SINE2pro::GFP-SINE1* construct.

Agrobacterium tumefaciens transformation

A. tumefaciens strain ABI was transformed with the corresponding constructs by triparental mating (Wise et al., 2006). In brief, the *Escherichia coli* carrying the constructs of interest were co-incubated overnight at 30°C on lysogeny broth agar (1.5%) plates with *A. tumefaciens* ABI and the *E. coli* helper strain containing the vector pRK2013. Then, the bacterial mixture was streaked on lysogeny broth agar (1.5%) plates with proper antibiotics to select transformed *A. tumefaciens*, which was confirmed by PCR.

N. benthamiana transient transformation

A. tumefaciens cultures containing plasmids expressing the proteins of interest were co-infiltrated transiently into *N. benthamiana* leaves as described previously (Sparkes et al., 2006). In brief, *A. tumefaciens* cultures were collected by centrifuging and resuspended to OD_{600} = 1.0 in the infiltration buffer containing 10 mM $MgCl_2$, 10 mM MES, pH 5.4, and 100 µM acetosyringone (Sigma-Aldrich). The *A. tumefaciens* suspension was pressure infiltrated into *N. benthamiana* leaves with a plastic syringe. Plants were grown for 2–3 d before being collected for the subsequence experiments.

A. thaliana stable transformation

Transgenic *A. thaliana* plants were obtained by *A. tumefaciens*–mediated floral dip (Clough and Bent, 1998). *A. tumefaciens* strains carrying the constructs of interest were inoculated in lysogeny broth liquid medium and grown overnight at 30°C. The bacteria were collected by centrifuging and resuspended in transformation solution containing 5% sucrose and 300 µl/liter Silwet L-77 (Lehle Seeds) to OD_{600} = 0.8. The inflorescence part of *A. thaliana* was dipped in the bacterial suspension. After being kept moist in the dark overnight at room temperature, the plants were moved to a growth chamber and allowed to set seeds. The transgenic plants were selected on Murashige and Skoog agar (0.8%) plates containing kanamycin or Basta (Sigma-Aldrich).

Co-IP experiments

N. benthamiana leaves were collected and ground in liquid nitrogen into powders, and co-IP experiments were performed at 4°C. 1 ml radioimmunoprecipitation assay buffer (50 mM Tris-HCl, pH 7.5, 150 mM NaCl, 0.1% SDS, 0.5% Na-deoxycholate, 1% NP-40, 1 mM PMSF, and 1% protease inhibitor cocktail [Sigma-Aldrich]) was used to extract 500 µl of plant tissue. One tenth of the protein extracts was used as the input sample, and the rest were used for IP using protein A–Sepharose beads (GE Healthcare) precoated with a rabbit anti-GFP antibody (ab290; Abcam). After 3× wash using radioimmunoprecipitation assay buffer, the immunoprecipitates and the input samples were separated by 8 or 10% SDS-PAGE, transferred to polyvinylidene difluoride membranes (Bio-Rad Laboratories), and detected with a mouse anti-GFP (1:2,000; 632569; Takara Bio Inc.) or a mouse anti-Myc (1:,000; M5546; Sigma-Aldrich) antibody. The input/IP ratio is 1:9.

Confocal microscopy and FRAP assay

7–10-d-old *A. thaliana* seedlings were imaged using a confocal microscope (Eclipse C90i; Nikon) with small or medium pinhole and gain setting range of 7.0–7.5. The 488-nm laser was set at 40% power for imaging *sun1-KO sun2-KD* transgenic plants whose transgene expression was low in all lines, whereas the other transgenic lines and *N. benthamiana* leaves were imaged using 10–20% laser power. All images were taken at room temperature using water as the medium with a Plan Apochromat VC 60× H lens (numerical aperture of 1.4; Nikon). The transmitted light detector was turned on to collect transmitted light signal simultaneously. Images were exported to PNG format by NIS-Elements software (Nikon) and organized in Photoshop and Illustrator (Adobe). The images shown in Fig. S3 A are 3D reconstitutions using NIS-Elements with the maximum projection blending option.

FRAP experiments were performed as described previously (Graumann et al., 2010; Zhou et al., 2012a) and conform to common membrane protein FRAP methodology (Shimi et al., 2004; Graumann et al., 2007; Östlund et al., 2009; Zuleger et al., 2011a; Martinière et al., 2012). The FRAP conditions as described as follows were identical for all experiments. In brief, a laser-scanning confocal microscope (510 Axiovert; Carl Zeiss) was used. Leaf sections of either transiently transformed *N. benthamiana* (Fig. 5) or stably transformed *A. thaliana* plants (Fig. 9 C and Fig. S4 C) were either directly mounted or first treated with 25 µM LatB for 30 min (or mock treated) before mounting. The 488-nm argon laser was used to excite GFP. For scanning, the laser transmission was kept below 5%, and for bleaching, it was used at 100%. The 63× oil immersion objective (numerical aperture 1.4) and a digital zoom factor of 2 were applied. Two differently sized regions of interest (ROIs) were used depending on nuclear size—for all FRAP experiments of *N. benthamiana* leaf epidermal cell nuclei, the ROI was always 51 µm^2, and for all FRAP experiments of *A. thaliana* leaf guard cell nuclei, the ROI was always 19 µm^2. For each sample, 35 nuclei were investigated. Fluorescent intensity in the ROI was observed—5 prebleach and 35 postbleach measurements were collected using the LSM browser (Carl Zeiss). For the bleach itself, approximately five iterations of the 100% 488-nm laser were used, which resulted in a 23–36% decrease of GFP fluorescence. Raw data were normalized onto a percentage scale using the equation $I_N = (I_T - I_{MIN})/(I_{MAX} - I_{MIN}) \times 100$, in which I_N is normalized fluorescence intensity, I_{MIN} is fluorescence intensity immediately after the bleach, and I_{MAX} is the mean prebleach fluorescence. Normalization was used to allow comparison and analysis of each individual FRAP experiment, as NE fluorescence is variable in both transiently and stably transformed cells. For each sample, the normalized data were

fitted to an exponential equation of best fit using Prism 4 (GraphPad Software), and half-time and maximum recovery were calculated. Statistical analysis was performed in Excel (Microsoft). The FRAP raw data are shown in Fig. S5.

RT-PCR analysis

Leaves of 20-d-old *A. thaliana* plants were ground in liquid nitrogen, and total RNA was extracted using RNeasy Plant Mini kit (QIAGEN). First-strand cDNA was synthesized using SuperScript III First-Strand Synthesis System (Life Technologies) and oligo-dT as a primer. Primers used for PCR were listed in Table S2.

GUS assays

A. thaliana seedlings were immersed in the GUS staining solution (0.1 M sodium phosphate buffer, pH 7.0, 10 mM EDTA, 0.1% [vol/vol] Triton X-100, 1 mM $K_3Fe(CN)_6$, and 2 mM X-Gluc [GoldBio]), vacuum infiltrated for 20 min, and incubated at 37°C for 3 h. Staining solution was then removed, and the seedlings were washed with several changes of 50% ethanol until the tissue was cleared. Seedlings were imaged under a dissecting microscope (C-LEDS; Nikon) or compound microscope (E100; Nikon) with a 10× lens (numerical aperture of 0.25) using water as a medium at room temperature. A camera (Omni ViD; OmniVision) was used to capture images, which were organized in Photoshop and Illustrator (Adobe).

Nuclear position measurement in guard cells

Leaves of 4–6-wk-old *A. thaliana* plants were used for the nuclear position measurement in guard cells. To open stomata, newly fully expanded leaves were detached, put on a piece of wet filter paper in a Petri dish, and irradiated with 100 µmol/m^2/s of blue light for 3 h. The lower epidermis was then peeled off and fixed and stained in 4% paraformaldehyde PBS buffer (137 mM NaCl, 2.7 mM KCl, 10 mM Na_2HPO_4, and 2 mM KH_2PO_4, pH 7.4) containing 4 µM Hoechst 33342 for ≥20 min. After this fixation and staining, the leaves were imaged using a digital camera (DS-Qi1Mc; Nikon). Leaves without blue light treatment were fixed, stained, and imaged in the same way, except for the *SINE1pro::GFP-SINE1* transformed *sine1-1* lines, which were imaged directly on a confocal microscope (C90i; Nikon) using the fluorescence from GFP-SINE1.

NIS-Elements software was used for the nuclear position measurement. An ellipse was first rendered on a pair of guard cells using the five-point ellipse tool. The major axis of the ellipse was aligned to the common boundary of the two guard cells. If the major axis was equal to or longer than 8 µm, the angles between the minor axis and the middle of the nuclei were measured using the free angle tool.

Hpa infection assay

A. thaliana seedlings were grown as described by Fabro et al. (2011). 10-d-old seedlings were sprayed with 3 × 10^5 spores/ml *Hpa* isolate Noco2 until the leaf surface was completely covered with spore solution. After infection, seedlings were kept for 6 d under a sealed transparent lid to maintain high humidity (~90–100%) at 17°C and 10/14-h day/night cycles. To quantify conidiophores, 40 seedlings per genotype were submerged in a solution of 0.1% Uvitex 2B (Polysciences, Inc.) followed by a wash in a 10× higher volume of water. Conidiophores emerging from the adaxial cotyledon side were counted using a fluorescent stereomicroscope (M165 FC; Leica) with a UV filter (Leica).

Online supplemental material

Fig. S1 shows amino acid sequence alignment of the C-terminal domains of WIP family members and a flow chart of DORY. Fig. S2 shows amino acid sequence alignment of the C-terminal domains of predicted KASH protein families not verified in this study. Fig. S3 shows expression pattern of SINE1 and SINE2 in leaves and roots. Fig. S4 shows that SINE1, but not SINE2, is associated with F-actin. Fig. S5 shows raw data of the FRAP analyses performed in this study. Table S1 provides primers used for cloning. Table S2 provides primers used for RT-PCR analyses and genotyping. The ZIP file provides a source code for the DORY program. The dataset shows corrected protein sequences used in the paper. Online supplemental material is available at http://www.jcb.org/cgi/content/full/jcb.201401138/DC1.

This work was funded by a grant from the National Science Foundation (MCB-1243844) to I. Meier. K. Graumann would like to acknowledge the Leverhulme Trust for her funding (ECF-2012-006). L. Wirthmueller and J.D.G. Jones acknowledge the Biotechnology and Biological Sciences Research Council (grant BB/K009176/1) and The Gatsby Charitable Foundation for funding.

The authors declare no competing financial interests.

Submitted: 30 January 2014
Accepted: 17 April 2014

References

Becker, B., and B. Marin. 2009. Streptophyte algae and the origin of embryophytes. *Ann. Bot. (Lond.)*. 103:999–1004. http://dx.doi.org/10.1093/aob/mcp044

Caillaud, M.-C., S.J.M. Piquerez, G. Fabro, J. Steinbrenner, N. Ishaque, J. Beynon, and J.D.G. Jones. 2012. Subcellular localization of the Hpa RxLR effector repertoire identifies a tonoplast-associated protein HaRxL17 that confers enhanced plant susceptibility. *Plant J.* 69:252–265. http://dx.doi.org/10.1111/j.1365-313X.2011.04787.x

Clough, S.J., and A.F. Bent. 1998. Floral dip: a simplified method for *Agrobacterium*-mediated transformation of *Arabidopsis thaliana*. *Plant J.* 16:735–743. http://dx.doi.org/10.1046/j.1365-313x.1998.00343.x

Coates, M.E., and J.L. Beynon. 2010. *Hyaloperonospora Arabidopsidis* as a pathogen model. *Annu. Rev. Phytopathol.* 48:329–345. http://dx.doi.org/10.1146/annurev-phyto-080508-094422

Crisp, M., Q. Liu, K. Roux, J.B. Rattner, C. Shanahan, B. Burke, P.D. Stahl, and D. Hodzic. 2006. Coupling of the nucleus and cytoplasm: role of the LINC complex. *J. Cell Biol.* 172:41–53. http://dx.doi.org/10.1083/jcb.200509124

de las Heras, J.I., P. Meinke, D.G. Batrakou, V. Srsen, N. Zuleger, A.R.W. Kerr, and E.C. Schirmer. 2013. Tissue specificity in the nuclear envelope supports its functional complexity. *Nucleus*. 4:460–477. http://dx.doi.org/10.4161/nucl.26872

Deslandes, L., and S. Rivas. 2011. The plant cell nucleus: a true arena for the fight between plants and pathogens. *Plant Signal. Behav.* 6:42–48. http://dx.doi.org/10.4161/psb.6.1.13978

De Souza, C.P.C., and S.A. Osmani. 2007. Mitosis, not just open or closed. *Eukaryot. Cell*. 6:1521–1527. http://dx.doi.org/10.1128/EC.00178-07

Elhanany-Tamir, H., Y.V. Yu, M. Shnayder, A. Jain, M. Welte, and T. Volk. 2012. Organelle positioning in muscles requires cooperation between two KASH proteins and microtubules. *J. Cell Biol.* 198:833–846. http://dx.doi.org/10.1083/jcb.201204102

Eun, S.O., and Y. Lee. 1997. Actin filaments of guard cells are reorganized in response to light and abscisic acid. *Plant Physiol.* 115:1491–1498. http://dx.doi.org/10.1104/pp.115.4.1491

Fabro, G., J. Steinbrenner, M. Coates, N. Ishaque, L. Baxter, D.J. Studholme, E. Körner, R.L. Allen, S.J. Piquerez, A. Rougon-Cardoso, et al. 2011. Multiple candidate effectors from the oomycete pathogen *Hyaloperonospora arabidopsidis* suppress host plant immunity. *PLoS Pathog.* 7:e1002348. http://dx.doi.org/10.1371/journal.ppat.1002348

Francis, K.E., S.Y. Lam, and G.P. Copenhaver. 2006. Separation of *Arabidopsis* pollen tetrads is regulated by QUARTET1, a pectin methylesterase gene. *Plant Physiol.* 142:1004–1013. http://dx.doi.org/10.1104/pp.106.085274

Goderis, I.J., M.F. De Bolle, I.E. François, P.F. Wouters, W.F. Broekaert, and B.P. Cammue. 2002. A set of modular plant transformation vectors allowing flexible insertion of up to six expression units. *Plant Mol. Biol.* 50:17–27. http://dx.doi.org/10.1023/A:1016052416053

Graumann, K., and D.E. Evans. 2010. The plant nuclear envelope in focus. *Biochem. Soc. Trans.* 38:307–311. http://dx.doi.org/10.1042/BST0380307

Graumann, K., and D.E. Evans. 2013. The nuclear envelope—structure and protein interactions. *In* Annual Plant Reviews. Vol. 46. D.E. Evans, K. Graumann, and J.A. Bryant, editors. John Wiley & Sons, Ltd., Oxford, England, UK. 19–55.

Graumann, K., S.L. Irons, J. Runions, and D.E. Evans. 2007. Retention and mobility of the mammalian lamin B receptor in the plant nuclear envelope. *Biol. Cell*. 99:553–562. http://dx.doi.org/10.1042/BC20070033

Graumann, K., J. Runions, and D.E. Evans. 2010. Characterization of SUN-domain proteins at the higher plant nuclear envelope. *Plant J.* 61:134–144. http://dx.doi.org/10.1111/j.1365-313X.2009.04038.x

Gross, P., C. Julius, E. Schmelzer, and K. Hahlbrock. 1993. Translocation of cytoplasm and nucleus to fungal penetration sites is associated with depolymerization of microtubules and defence gene activation in infected, cultured parsley cells. *EMBO J.* 12:1735–1744.

Gruenbaum, Y., R.D. Goldman, R. Meyuhas, E. Mills, A. Margalit, A. Fridkin, Y. Dayani, M. Prokocimer, and A. Enosh. 2003. The nuclear lamina and its functions in the nucleus. *Int. Rev. Cytol.* 226:1–62. http://dx.doi.org/10.1016/S0074-7696(03)01001-5

Guest, D.I. 1986. Evidence from light microscopy of living tissues that Fosetyl-Al modifies the defence response in tobacco seedlings following inoculation by *Phytophthora nicotianae* var *nicotianae*. *Physiol. Mol. Plant Pathol.* 29:251–261. http://dx.doi.org/10.1016/S0048-4059(86)80025-X

Gundersen, G.G., and H.J. Worman. 2013. Nuclear positioning. *Cell*. 152:1376–1389. http://dx.doi.org/10.1016/j.cell.2013.02.031

Hampoelz, B., and T. Lecuit. 2011. Nuclear mechanics in differentiation and development. *Curr. Opin. Cell Biol.* 23:668–675. http://dx.doi.org/10.1016/j.ceb.2011.10.001

Higaki, T., N. Kutsuna, T. Sano, N. Kondo, and S. Hasezawa. 2010. Quantification and cluster analysis of actin cytoskeletal structures in plant cells: role of actin bundling in stomatal movement during diurnal cycles in *Arabidopsis* guard cells. *Plant J.* 61:156–165. http://dx.doi.org/10.1111/j.1365-313X.2009.04032.x

Horn, H.F., D.I. Kim, G.D. Wright, E.S. Wong, C.L. Stewart, B. Burke, and K.J. Roux. 2013. A mammalian KASH domain protein coupling meiotic chromosomes to the cytoskeleton. *J. Cell Biol.* 202:1023–1039. http://dx.doi.org/10.1083/jcb.201304004

Hwang, Y.T., S.M. Pelitire, M.P.A. Henderson, D.W. Andrews, J.M. Dyer, and R.T. Mullen. 2004. Novel targeting signals mediate the sorting of different isoforms of the tail-anchored membrane protein cytochrome b5 to either endoplasmic reticulum or mitochondria. *Plant Cell*. 16:3002–3019. http://dx.doi.org/10.1105/tpc.104.026039

Jiang, K., K. Sorefan, M.J. Deeks, M.W. Bevan, P.J. Hussey, and A.M. Hetherington. 2012. The ARP2/3 complex mediates guard cell actin reorganization and stomatal movement in *Arabidopsis*. *Plant Cell*. 24:2031–2040. http://dx.doi.org/10.1105/tpc.112.096263

Käll, L., A. Krogh, and E.L. Sonnhammer. 2007. Advantages of combined transmembrane topology and signal peptide prediction—the Phobius web server. *Nucleic Acids Res.* 35(Suppl. 2):W429–W432. http://dx.doi.org/10.1093/nar/gkm256

Karimi, M., D. Inzé, and A. Depicker. 2002. GATEWAY vectors for *Agrobacterium*-mediated plant transformation. *Trends Plant Sci.* 7:193–195. http://dx.doi.org/10.1016/S1360-1385(02)02251-3

Katoh, K., and D.M. Standley. 2013. MAFFT multiple sequence alignment software version 7: improvements in performance and usability. *Mol. Biol. Evol.* 30:772–780. http://dx.doi.org/10.1093/molbev/mst010

Ketema, M., K. Wilhelmsen, I. Kuikman, H. Janssen, D. Hodzic, and A. Sonnenberg. 2007. Requirements for the localization of nesprin-3 at the nuclear envelope and its interaction with plectin. *J. Cell Sci.* 120:3384–3394. http://dx.doi.org/10.1242/jcs.014191

Korfali, N., G.S. Wilkie, S.K. Swanson, V. Srsen, J.I. de Las Heras, D.G. Batrakou, P. Malik, N. Zuleger, A.R.W. Kerr, L. Florens, and E.C. Schirmer. 2012. The nuclear envelope proteome differs notably between tissues. *Nucleus*. 3:552–564. http://dx.doi.org/10.4161/nucl.22257

Li, L.-J., F.E.I. Ren, X.-Q. Gao, P.-C. Wei, and X.-C. Wang. 2013. The reorganization of actin filaments is required for vacuolar fusion of guard cells during stomatal opening in *Arabidopsis*. *Plant Cell Environ.* 36:484–497. http://dx.doi.org/10.1111/j.1365-3040.2012.02592.x

Lindeman, R.E., and F. Pelegri. 2012. Localized products of *futile cycle/lrmp* promote centrosome-nucleus attachment in the zebrafish zygote. *Curr. Biol.* 22:843–851. http://dx.doi.org/10.1016/j.cub.2012.03.058

Luxton, G.W., E.R. Gomes, E.S. Folker, E. Vintinner, and G.G. Gundersen. 2010. Linear arrays of nuclear envelope proteins harness retrograde actin flow for nuclear movement. *Science*. 329:956–959. http://dx.doi.org/10.1126/science.1189072

MacRobbie, E.A.C., and S. Kurup. 2007. Signalling mechanisms in the regulation of vacuolar ion release in guard cells. *New Phytol.* 175:630–640. http://dx.doi.org/10.1111/j.1469-8137.2007.02131.x

Malone, C.J., W.D. Fixsen, H.R. Horvitz, and M. Han. 1999. UNC-84 localizes to the nuclear envelope and is required for nuclear migration and anchoring during *C. elegans* development. *Development*. 126:3171–3181.

Martinière, A., I. Lavagi, G. Nageswaran, D.J. Rolfe, L. Maneta-Peyret, D.-T. Luu, S.W. Botchway, S.E.D. Webb, S. Mongrand, C. Maurel, et al. 2012. Cell wall constrains lateral diffusion of plant plasma-membrane proteins. *Proc. Natl. Acad. Sci. USA*. 109:12805–12810. http://dx.doi.org/10.1073/pnas.1202040109

McGee, M.D., I. Stagljar, and D.A. Starr. 2009. KDP-1 is a nuclear envelope KASH protein required for cell-cycle progression. *J. Cell Sci.* 122:2895–2905. http://dx.doi.org/10.1242/jcs.051607

Meier, I. 2001. The plant nuclear envelope. *Cell. Mol. Life Sci.* 58:1774–1780. http://dx.doi.org/10.1007/PL00000817

Meier, I., X.M. Xu, J. Brkljacic, Q. Zhao, and H.J. Wang. 2008. Going green: plants' alternative way to position the Ran gradient. *J. Microsc.* 231:225–233. http://dx.doi.org/10.1111/j.1365-2818.2008.02038.x

Mekhail, K., and D. Moazed. 2010. The nuclear envelope in genome organization, expression and stability. *Nat. Rev. Mol. Cell Biol.* 11:317–328. http://dx.doi.org/10.1038/nrm2894

Mellad, J.A., D.T. Warren, and C.M. Shanahan. 2011. Nesprins LINC the nucleus and cytoskeleton. *Curr. Opin. Cell Biol.* 23:47–54. http://dx.doi.org/10.1016/j.ceb.2010.11.006

Morimoto, A., H. Shibuya, X. Zhu, J. Kim, K. Ishiguro, M. Han, and Y. Watanabe. 2012. A conserved KASH domain protein associates with telomeres, SUN1, and dynactin during mammalian meiosis. *J. Cell Biol.* 198:165–172. http://dx.doi.org/10.1083/jcb.201204085

Nakagawa, T., T. Kurose, T. Hino, K. Tanaka, M. Kawamukai, Y. Niwa, K. Toyooka, K. Matsuoka, T. Jinbo, and T. Kimura. 2007. Development of series of gateway binary vectors, pGWBs, for realizing efficient construction of fusion genes for plant transformation. *J. Biosci. Bioeng.* 104:34–41. http://dx.doi.org/10.1263/jbb.104.34

Neumann, N., D. Lundin, and A.M. Poole. 2010. Comparative genomic evidence for a complete nuclear pore complex in the last eukaryotic common ancestor. *PLoS ONE*. 5:e13241. http://dx.doi.org/10.1371/journal.pone.0013241

Oda, Y., and H. Fukuda. 2011. Dynamics of *Arabidopsis* SUN proteins during mitosis and their involvement in nuclear shaping. *Plant J.* 66:629–641. http://dx.doi.org/10.1111/j.1365-313X.2011.04523.x

Östlund, C., E.S. Folker, J.C. Choi, E.R. Gomes, G.G. Gundersen, and H.J. Worman. 2009. Dynamics and molecular interactions of linker of nucleoskeleton and cytoskeleton (LINC) complex proteins. *J. Cell Sci.* 122:4099–4108. http://dx.doi.org/10.1242/jcs.057075

Padmakumar, V.C., T. Libotte, W. Lu, H. Zaim, S. Abraham, A.A. Noegel, J. Gotzmann, R. Foisner, and I. Karakesisoglou. 2005. The inner nuclear membrane protein Sun1 mediates the anchorage of Nesprin-2 to the nuclear envelope. *J. Cell Sci.* 118:3419–3430. http://dx.doi.org/10.1242/jcs.02471

Razafsky, D., and D. Hodzic. 2009. Bringing KASH under the SUN: the many faces of nucleo-cytoskeletal connections. *J. Cell Biol.* 186:461–472. http://dx.doi.org/10.1083/jcb.200906068

Reits, E.A.J., and J.J. Neefjes. 2001. From fixed to FRAP: measuring protein mobility and activity in living cells. *Nat. Cell Biol.* 3:E145–E147. http://dx.doi.org/10.1038/35078615

Riedl, J., A.H. Crevenna, K. Kessenbrock, J.H. Yu, D. Neukirchen, M. Bista, F. Bradke, D. Jenne, T.A. Holak, Z. Werb, et al. 2008. Lifeact: a versatile marker to visualize F-actin. *Nat. Methods*. 5:605–607. http://dx.doi.org/10.1038/nmeth.1220

Rothballer, A., and U. Kutay. 2013. The diverse functional LINCs of the nuclear envelope to the cytoskeleton and chromatin. *Chromosoma*. 122:415–429. http://dx.doi.org/10.1007/s00412-013-0417-x

Roux, K.J., M.L. Crisp, Q. Liu, D. Kim, S. Kozlov, C.L. Stewart, and B. Burke. 2009. Nesprin 4 is an outer nuclear membrane protein that can induce kinesin-mediated cell polarization. *Proc. Natl. Acad. Sci. USA*. 106:2194–2199. http://dx.doi.org/10.1073/pnas.0808602106

Schmelzer, E. 2002. Cell polarization, a crucial process in fungal defence. *Trends Plant Sci.* 7:411–415. http://dx.doi.org/10.1016/S1360-1385(02)02307-5

Schreiber, K.H., and B.K. Kennedy. 2013. When lamins go bad: nuclear structure and disease. *Cell*. 152:1365–1375. http://dx.doi.org/10.1016/j.cell.2013.02.015

Shimi, T., T. Koujin, M. Segura-Totten, K.L. Wilson, T. Haraguchi, and Y. Hiraoka. 2004. Dynamic interaction between BAF and emerin revealed by FRAP, FLIP, and FRET analyses in living HeLa cells. *J. Struct. Biol.* 147:31–41. http://dx.doi.org/10.1016/j.jsb.2003.11.013

Skalamera, D., and M.C. Heath. 1998. Changes in the cytoskeleton accompanying infection-induced nuclear movements and the hypersensitive response in plant cells invaded by rust fungi. *Plant J.* 16:191–200. http://dx.doi.org/10.1046/j.1365-313x.1998.00285.x

Sosa, B.A., A. Rothballer, U. Kutay, and T.U. Schwartz. 2012. LINC complexes form by binding of three KASH peptides to domain interfaces of trimeric SUN proteins. *Cell*. 149:1035–1047. http://dx.doi.org/10.1016/j.cell.2012.03.046

Sparkes, I.A., J. Runions, A. Kearns, and C. Hawes. 2006. Rapid, transient expression of fluorescent fusion proteins in tobacco plants and generation of stably transformed plants. *Nat. Protoc.* 1:2019–2025. http://dx.doi.org/10.1038/nprot.2006.286

Starr, D.A., and H.N. Fridolfsson. 2010. Interactions between nuclei and the cytoskeleton are mediated by SUN-KASH nuclear-envelope bridges. *Annu. Rev. Cell Dev. Biol.* 26:421–444. http://dx.doi.org/10.1146/annurev-cellbio-100109-104037

Starr, D.A., G.J. Hermann, C.J. Malone, W. Fixsen, J.R. Priess, H.R. Horvitz, and M. Han. 2001. *unc-83* encodes a novel component of the nuclear envelope and is essential for proper nuclear migration. *Development*. 128:5039–5050.

Tamura, K., K. Iwabuchi, Y. Fukao, M. Kondo, K. Okamoto, H. Ueda, M. Nishimura, and I. Hara-Nishimura. 2013. Myosin XI-i links the nuclear membrane to the cytoskeleton to control nuclear movement and shape in *Arabidopsis*. *Curr. Biol.* 23:1776–1781. http://dx.doi.org/10.1016/j.cub.2013.07.035

Wise, A.A., Z. Liu, and A.N. Binns. 2006. Three methods for the introduction of foreign DNA into *Agrobacterium*. *Methods Mol. Biol.* 343:43–53.

Xu, X.M., T. Meulia, and I. Meier. 2007. Anchorage of plant RanGAP to the nuclear envelope involves novel nuclear-pore-associated proteins. *Curr. Biol.* 17:1157–1163. http://dx.doi.org/10.1016/j.cub.2007.05.076

Zhang, X., K. Lei, X. Yuan, X. Wu, Y. Zhuang, T. Xu, R. Xu, and M. Han. 2009. SUN1/2 and Syne/Nesprin-1/2 complexes connect centrosome to the nucleus during neurogenesis and neuronal migration in mice. *Neuron*. 64:173–187. http://dx.doi.org/10.1016/j.neuron.2009.08.018

Zhao, Q., J. Brkljacic, and I. Meier. 2008. Two distinct interacting classes of nuclear envelope-associated coiled-coil proteins are required for the tissue-specific nuclear envelope targeting of *Arabidopsis* RanGAP. *Plant Cell*. 20:1639–1651. http://dx.doi.org/10.1105/tpc.108.059220

Zhou, X., and I. Meier. 2013. How plants LINC the SUN to KASH. *Nucleus*. 4:206–215. http://dx.doi.org/10.4161/nucl.24088

Zhou, X., K. Graumann, D.E. Evans, and I. Meier. 2012a. Novel plant SUN–KASH bridges are involved in RanGAP anchoring and nuclear shape determination. *J. Cell Biol.* 196:203–211. http://dx.doi.org/10.1083/jcb.201108098

Zhou, Z.C., X.L. Du, Z. Cai, X.M. Song, H.T. Zhang, T. Mizuno, E. Suzuki, M.R. Yee, A. Berezov, R. Murali, et al. 2012b. Structure of Sad1-UNC84 homology (SUN) domain defines features of molecular bridge in nuclear envelope. *J. Biol. Chem.* 287:5317–5326. http://dx.doi.org/10.1074/jbc.M111.304543

Zuleger, N., D.A. Kelly, A.C. Richardson, A.R.W. Kerr, M.W. Goldberg, A.B. Goryachev, and E.C. Schirmer. 2011a. System analysis shows distinct mechanisms and common principles of nuclear envelope protein dynamics. *J. Cell Biol.* 193:109–123. http://dx.doi.org/10.1083/jcb.201009068

Zuleger, N., M.I. Robson, and E.C. Schirmer. 2011b. The nuclear envelope as a chromatin organizer. *Nucleus*. 2:339–349. http://dx.doi.org/10.4161/nucl.2.5.17846